Lithos 384–385 (2021) 105976

Contents lists available at ScienceDirect

Lithos

journal homepage: www.elsevier.com/locate/lithos

Research Article

Tracking halogen recycling and volatile loss in kimberlite magmatism from Greenland: Evidence from combined F-Cl-Br and $\delta^{37}Cl$ systematics

Brendan C. Hoare [a,*], Emma L. Tomlinson [a], Jaime D. Barnes [b], Sebastian Tappe [c], Michael A.W. Marks [d], Tatjana Epp [d], John Caulfield [e], Thomas Riegler [a]

[a] Department of Geology, Trinity College Dublin, Dublin 2, Ireland
[b] Department of Geological Sciences, University of Texas, Austin, TX 78712, USA
[c] Deep & Early Earth Processes (DEEP) Research Group, Department of Geology, University of Johannesburg, 2006 Auckland Park, South Africa
[d] Department of Geosciences, Eberhard Karls University, Schnarrenbergstr. 94 + 96, 72076 Tübingen, Germany
[e] Central Analytical Research Facility, Queensland University of Technology, Brisbane 4000, QLD, Australia

ARTICLE INFO

Article history:
Received 15 June 2020
Received in revised form 7 December 2020
Accepted 5 January 2021
Available online 08 January 2021

ABSTRACT

Kimberlite magmatism occurs as a result of volatile fluxed melting of the convecting upper mantle underlying cratonic lithospheric mantle regions. During passage to the Earth's surface, proto-kimberlite magma can interact with, and assimilate, variably enriched cratonic mantle producing hybrid melts consisting of asthenospheric and cratonic mantle components including contributions from metasomatic domains. The halogen elements (F, Cl, Br, I) and chlorine isotope ratios ($^{37}Cl/^{35}Cl$) are increasingly used as tracers of recycled crustal materials within the Earth's mantle yet are only rarely reported in analyses of kimberlites. As a result, the origin and distribution of halogens in kimberlite magmas is poorly constrained. Here, we present novel, combined elemental (F, Cl, Br) and isotopic ($\delta^{37}Cl$) halogen data for 14 fresh kimberlite samples from the North Atlantic Craton (NAC) of West and South-West Greenland.

The F composition of kimberlites from the NAC appears to be controlled by melting in the convecting upper mantle with minimal effect from interaction with metasomatized lithospheric mantle or volatile loss during or after emplacement. By contrast, Cl and Br in the studied samples have undergone significant devolatilization during kimberlite dyke emplacement and post-emplacement processes, whereby up to 99% of the original halogen budget was removed.

Whilst all the studied kimberlites broadly follow the same geochemical pattern, there exists some regional variability in their halogen systematics. The northern NAC kimberlite samples from Majuagaa have mantle-like $\delta^{37}Cl$ values of −0.2 to −0.5‰ [versus SMOC (standard mean ocean chloride)]. In contrast, kimberlite dykes from Nigerdlikasik and Pyramidefjeld near the southern craton margin display positive $\delta^{37}Cl$ values of +0.4‰ to +1.3‰, in addition to a relative Cl and Br enrichment, which is consistent with the assimilation of recycled crust-derived halogens by the kimberlite magmas. The data support a scenario in which recycled halogens were sampled either from within an OIB-type reservoir in the convecting mantle or through interaction with subduction-modified lithospheric mantle reservoir during eruption. We prefer a scenario in which the ascending kimberlite magmas assimilated Cl-rich, metasomatized regions within cratonic mantle lithosphere.

1. Introduction

Although relatively minor constituents of continental magmatism, kimberlites garner significant interest due to their hosting of diamonds and mantle xenoliths scavenged from great depths during magma ascent. Kimberlites and related magmas are thought to form by low-degree melting of the convecting Earth's mantle in intra-continental settings where the lithosphere is particularly thick, at depths in excess of 150 km (Brey et al., 2008; Dalton and Presnall, 1998; Foley et al., 2019). The high MgO, NiO, and incompatible trace element contents of kimberlites are best explained as a result of low-degree partial melting of carbonated peridotite within the convecting ambient upper mantle (e.g. Tappe et al., 2018), although deep mantle plume sources have also been invoked (e.g. le Roex, 1986; Tachibana et al., 2006). These varieties of magmatism display extremely high concentrations of incompatible trace elements in addition to extreme concentrations of volatiles such as H_2O and CO_2 (Kjarsgaard et al., 2009). Compared to the relatively well-studied (if still not fully understood) volatiles H_2O and CO_2, concentrations of the halogens F and Cl are only rarely

* Corresponding author.
E-mail address: hoareb@tcd.ie (B.C. Hoare).

https://doi.org/10.1016/j.lithos.2021.105976

reported for kimberlites (Abersteiner et al., 2017; Kjarsgaard et al., 2009), and Br data are lacking entirely. Hence, the origins and distributions of halogens in kimberlite magmas are only poorly constrained.

During their ascent to the Earth's surface, kimberlite magmas can interact with, as well as mechanically entrain, variably enriched cratonic mantle materials leading to the production of hybrid magmas containing sub-lithospheric and lithospheric mantle components (e.g. Mitchell, 2008; Dalton et al., 2020; Giuliani et al., 2020). Volatiles introduced into the continental mantle via metasomatism are postulated to derive from fluids/melts released from subducted slabs of oceanic lithosphere (Bell et al., 2005; Broadley et al., 2016; Simon et al., 2007; Wang et al., 2016) or directly from the asthenosphere by low-degree partial melts (Aulbach et al., 2013; Grégoire et al., 2002, 2003; le Roex and Class, 2016; Rudnick et al., 1993; Tappe et al., 2017; Yaxley et al., 1991). As a result, kimberlites can diverge in composition as a function of the degree of craton enrichment and intensity of assimilation but also the sampling of OIB-type reservoirs in their source regions, as evidenced by their variable major and trace element contents, and radiogenic isotope (Sr-Nd-Hf-Pb-Os) compositions (Chalapathi Rao et al., 2013; Foley et al., 2019; le Roex et al., 2003; Pearson et al., 2019; Tappe et al., 2011a; Tappe et al., 2020b).

The halogen elements (F, Cl, Br) as well as the chlorine isotope system ($^{37}Cl/^{35}Cl$) could offer significant potential for distinguishing metasomatic styles in the cratonic lithosphere and tracing recycled volatiles in the kimberlite magma source region, because they have been established as valuable tracers of recycled crustal material in the Earth's mantle for other less complex magmatic and metamorphic systems (Broadley et al., 2016; Broadley et al., 2019; Halldórsson et al., 2016; John et al., 2010; Kendrick et al., 2012b; Kendrick et al., 2017). Whilst it is expected that sampling of recycled halogens either from within the convecting mantle (i.e. from OIB reservoirs) or metasomatized cratonic lithosphere could potentially influence the halogen content of ascending kimberlite magmas, the influence of either such reservoirs on the composition of kimberlite magmas is unproven. This results in part from the difficulty in ascertaining the halogen contents of kimberlite magmas, which is hampered by the effects of volatile loss via exsolution during ascent and emplacement, as well as post-emplacement alteration (Abersteiner et al., 2017). Studies of melt inclusions in kimberlite magmas show a multitude of halogen-bearing phases, which implies that halogens are common constituents of primitive kimberlite magmas (e.g. Abersteiner et al., 2017, 2019b; Kamenetsky et al., 2014). Yet the magmas themselves have halogen contents (F, Cl) that are broadly similar to MORB and OIB magmas (Kendrick et al., 2017; Kjarsgaard et al., 2009). However, the degree to which halogen loss occurs during kimberlite magmatism remains poorly constrained.

Here, we provide the first combined elemental (F, Cl, Br) and isotopic ($\delta^{37}Cl$) investigation of the halogen inventory of kimberlite magmas with the aim to estimate their original halogen contents. This study also seeks to understand the underlying mechanisms by which the observed regionally diverging halogen compositions of kimberlites from Greenland are created.

2. Samples and geological setting

2.1. Selected samples

This study focuses on 14 hypabyssal kimberlite samples from the northern (Majuagaa), central (Tikiusaaq), and southern (Nigerdlikasik and Pyramidefjeld) regions of the NAC in West and South-West Greenland (Fig. 1). In addition, we analyzed the concentrations of chlorine in serpentine veins within spinel- and phlogopite-bearing peridotite xenoliths ($n = 6$) recovered from kimberlite dykes at Nigerdlikasik and Pyramidefjeld. Two of these xenoliths (P3580-X1; P3581-X1) were coarsely crushed and hand-picked for phlogopite. Phlogopite was crushed and aliquots were analyzed for their halogen concentrations. P3581-X1 was also analyzed for its $\delta^{37}Cl$ isotope composition.

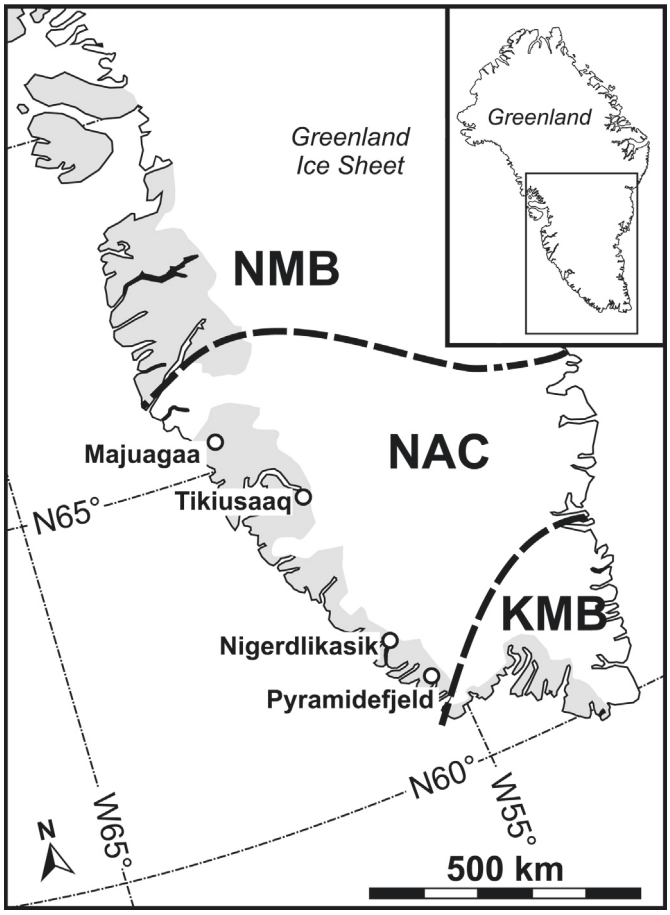

Fig. 1. Location of the Majuagaa, Tikiusaaq, Nigerdlikasik and Pyramidefjeld kimberlites on the now rifted North Atlantic Craton (NAC). NMB - Nagsuqtoqidian mobile belt; KMB - Ketilidian mobile belt.

Kimberlite samples analyzed in this study from the northern NAC are sampled from the Majuagaa kimberlite dyke part of the wider Maniitsoq kimberlite field. Kimberlite dykes from the Maniitsoq field are isotopically moderately depleted (Tappe et al., 2011a), with Sr-Nd-Hf isotopic compositions that overlap with archetypal group-I kimberlites from southern Africa (Nowell et al., 2004; Smith, 1983; Tappe et al., 2020a), suggesting a source in the convecting ambient upper mantle to transition zone. A dominantly convective upper mantle source is supported by low K_2O contents (0.06–0.3 wt% K_2O), which suggests minimal interaction with metasomatized cratonic mantle domains. Kimberlite dykes from the Maniitsoq region yield ages between 568 and 553 Ma (Tappe et al., 2011a, 2011b). For detailed field relations and petrographic descriptions see Nielsen and Sand (2008) and Nielsen et al. (2009).

Ultramafic carbonate-rich dykes were emplaced in the center of the NAC at Tikiusaaq at around 160 Ma and, similar to the Maniitsoq kimberlite dykes, are interpreted to derive from the convective upper mantle based on their Sr-Nd-Hf-Pb-Li isotopic compositions (Tappe et al., 2012, 2017). They have relatively enriched K_2O compositions (0.92–1.40 wt% K_2O) compared to kimberlites from Maniitsoq and can be considered transitional between calcite kimberlite and aillikite - the carbonate-rich ultramafic lamprophyre end-member variety (Tappe et al., 2005). The higher K_2O contents of magmas at Tikiusaaq, compared to those at Maniitsoq, imply that Tikiusaaq kimberlite magmas could have assimilated minor amounts of a K-bearing phase, either K-richterite or phlogopite, during passage through the cratonic mantle. The high K/Na ratios and silica-undersaturation of magmas at Tikiusaaq suggest that phlogopite is the most likely source of K-enrichment. The

depleted $^{87}Sr/^{86}Sr$ isotope character of the Tikiusaaq kimberlite dykes requires that phlogopite was added to the cratonic mantle only shortly prior to kimberlite magmatism recorded at surface (Tappe et al., 2017). U–Pb dating of groundmass perovskite provides emplacement ages of between 157.4 and 165.9 Ma for the Tikiusaaq kimberlite dykes (Tappe et al., 2012). For detailed field relations plus petrographic and mineralogical descriptions of the samples used in this study see Steenfelt et al. (2006) and Tappe et al. (2009).

Ultramafic carbonate-rich magmas from the southern margin of the NAC are represented by two dykes from Nigerdlikasik and a sill from Østragrav, which is part of the wider Pyramidefjeld-Midternaes kimberlite field first reported in detail by Emeleus and Andrews (1975). Similar to Tikiusaaq, the dyke/sheet intrusions at Nigerdlikasik can be considered transitional between calcite kimberlite and aillikite, whilst those from Pyramidefjeld are aillikite sensu stricto given the presence of ubiquitous groundmass clinopyroxene (Emeleus and Andrews, 1975; Larsen and Rex, 1992; Tappe et al., 2005). For simplicity we group them as kimberlites hereafter. As with samples from Tikiusaaq, the relatively high K_2O (1.28–1.66 wt% K_2O) contents of magmas from Pyramidefjeld and Nigerdlikasik imply assimilation of phlogopite en route to the surface. Kimberlite magmatism at Pyramidefjeld-Midternaes is dated to ca. 150 Ma by U/Pb perovskite geochronology (Larsen et al., 2009), but no high-precision age data exist for the Nigerdlikasik kimberlite. However, early attempts to date the kimberlites at Nigerdlikasik and Pyramidefjeld with the K–Ar method revealed that these dyke occurrences are broadly coeval (Andrews and Emeleus, 1971; Bridgwater, 1970). Therefore, it is reasonable to conclude that the kimberlite magmatism at Nigerdlikasik, Pyramidefjeld, and Tikiusaaq was broadly coeval between 165 and 150 Ma, largely controlled by the development of nearby continental rift basins off the present-day West Greenland coast (Hansen, 1980; Larsen et al., 2009; Tappe et al., 2007, 2017).

2.2. Kimberlite and xenolith petrography

The hypabyssal dyke samples from Majuagaa, Tikiusaaq, Nigerdlikasik and Pyramidefjeld have a typical calcite kimberlite to aillikite primary mineralogy (Mitchell, 1986; Tappe et al., 2005) displaying a hybrid petrography due to the presence of mantle-derived xenocrysts (Mitchell, 2008). Although hypabyssal kimberlites are frequently thought to be undegassed or to have undergone only limited amounts of degassing (e.g. Mitchell, 2008), recent experiments and modeling studies on natural sample suites indicate that kimberlite dykes may have lost up to 20 wt% CO_2 upon magma emplacement (Brooker et al., 2011; Dongre and Tappe, 2019).

In kimberlites from the NAC used in this study, olivine is the most common macrocryst (up to 30 vol%) except for the Tikiusaaq kimberlites, where it is only rarely seen. Where present, macrocrystic olivine appears as two distinct populations, as previously recognized for kimberlites and aillikites from localities worldwide on the basis of petrography and compositions (Bussweiler et al., 2015; Kamenetsky et al., 2008; Rooney et al., 2020). The first and most common population comprises rounded anhedral olivine often partially serpentinized, which is interpreted as entrained from the lithospheric mantle (i.e. xenocrysts) during magma ascent. The second olivine population comprises sub- to euhedral grains that are generally much smaller and interpreted as magmatic crystallization product. Macrocrystic phlogopite occurs in all samples as scant euhedral laths. In the Majuagaa kimberlite, rare xenocrystic garnet, diopside and 'corroded or dusty' orthopyroxene are also present (Nielsen and Sand, 2008).

The groundmass of samples from Majuagaa, Nigerdlikasik and Pyramidefjeld is similar and consists of calcite/dolomite and serpentine, common to most hypabyssal kimberlites globally (Mitchell, 2013). In kimberlites from Nigerdlikasik and Pyramidefjeld serpentine occurs as partially or completely replaced pseudomorphs after olivine. The serpentine pseudomorphs are not infiltrated by later interstitial serpentine within the groundmass implying an earlier phase of serpentinization within the kimberlite magma. Olivine within the samples from the Maniitsoq field display negligible serpentinization compared that seen in olivine from Nigerdlikasik or Pyramidefjeld (Nielsen and Sand, 2008).

It is inferred that the serpentine and carbonate groundmass crystallized together from volatile-rich ($CO_2 + H_2O$) deuteric residua as a polycrystalline mesostasis or in discrete segregations (Mitchell, 2008). However, an additional influx of externally derived meteoric fluids has also been invoked in the origin of the groundmass of hypabyssal kimberlites (Giuliani et al., 2014; Sparks et al., 2009; Wilson et al., 2007). No evidence of substantial subaerial weathering is observed in any of the kimberlite samples from Greenland. Samples from Tikiusaaq are almost completely serpentine free, which is common in H_2O-poor and carbonate-rich hypabyssal kimberlites and aillikites (Tappe et al., 2009), such as the Udachnaya-East kimberlite from the Siberian craton (e.g. Kamenetsky et al., 2007, 2014) and the Benfontein kimberlite sills on the Kaapvaal craton (Dawson and Hawthorne, 1973).

Accessory groundmass phases are typically <50 μm, mainly comprising perovskite, rutile, ilmenite, spinel, pyrite, diopside and apatite. In the kimberlite from Pyramidefjeld primary serpentine comprises the majority of the groundmass with carbonate being a less common constituent, whilst the opposite is true for kimberlites from Nigerdlikasik, i.e. carbonate predominates the groundmass. It appears the kimberlites from Nigerdlikasik and Majuagaa are intermediate in terms of serpentine content between samples from 'serpentine-rich' kimberlite at Pyramidefjeld and 'serpentine-poor' kimberlites at Tikiusaaq.

Mantle xenoliths used in this study from the southern margin of the NAC are phlogopite-rich dunite, harzburgite and wehrlite. Representative xenoliths are shown in Fig. 2c-d.

2.3. Geological setting

The main phase of lithosphere formation and stabilization in the north and center of the NAC took place between 3.2 and 2.8 Ga, as suggested by the mode of Re–Os model ages for cratonic mantle peridotite xenoliths recovered from the northern parts of the NAC at Maniitsoq and Sarfartoq (Wittig et al., 2010). Meso- to Neoarchean lithospheric mantle root stabilization ages are common to a number of cratons worldwide (Irvine et al., 2003; Pearson et al., 1995a, 1995b) and for the NAC they match well with the main phase of tonalite-trondhjemite-granodiorite (TTG) and granite crust formation between 3.1 and 2.9 Ga (e.g. Nutman et al., 2004), as well as with 2.9 ± 0.3 Ga subducted eclogite components that are vestiges of the collisions by which the NAC grew (Tappe et al., 2011b). The relatively narrow spread in Re–Os model ages for the sub-continental lithospheric mantle of the northern and central NAC suggests that relatively little metasomatic overprinting has occurred (van Acken et al., 2017; Wittig et al., 2010), a situation that appears to be different for the southern parts of the NAC from where extensive metasomatism has been reported (Aulbach et al., 2017, 2019; Goodenough et al., 2002). For example, platinum-group element (PGE) systematics of mantle peridotites from the southern margin of the NAC at Pyramidefjeld are distinctly overprinted resulting from refertilization of the mantle lithosphere at ca. 2.1–1.8 Ga possibly concomitant with the assembly of Laurentia and during later recurrent rifting of the NAC throughout its post-Archean evolution (Aulbach et al., 2019; Wittig et al., 2010).

Paleoproterozoic subduction-related metasomatism of the cratonic mantle along the southern NAC margin is suggested by trace element systematics of ca. 1.2 Ga basaltic magmatism of the Mesoproterozoic (ca. 1.3 Ga) Gardar province on the southernmost NAC and neighboring Ketilidian mobile belt (Goodenough et al., 2002). Late Gardar (~1.3 Ga) basaltic magmatism is thought to have from formed by large-scale decompression melting of enriched cratonic mantle that produced melts displaying pronounced high-field strength element anomalies and light rare-earth element and large-ion lithophile element enrichments (Bartels et al., 2015; Goodenough et al., 2002), characteristic of

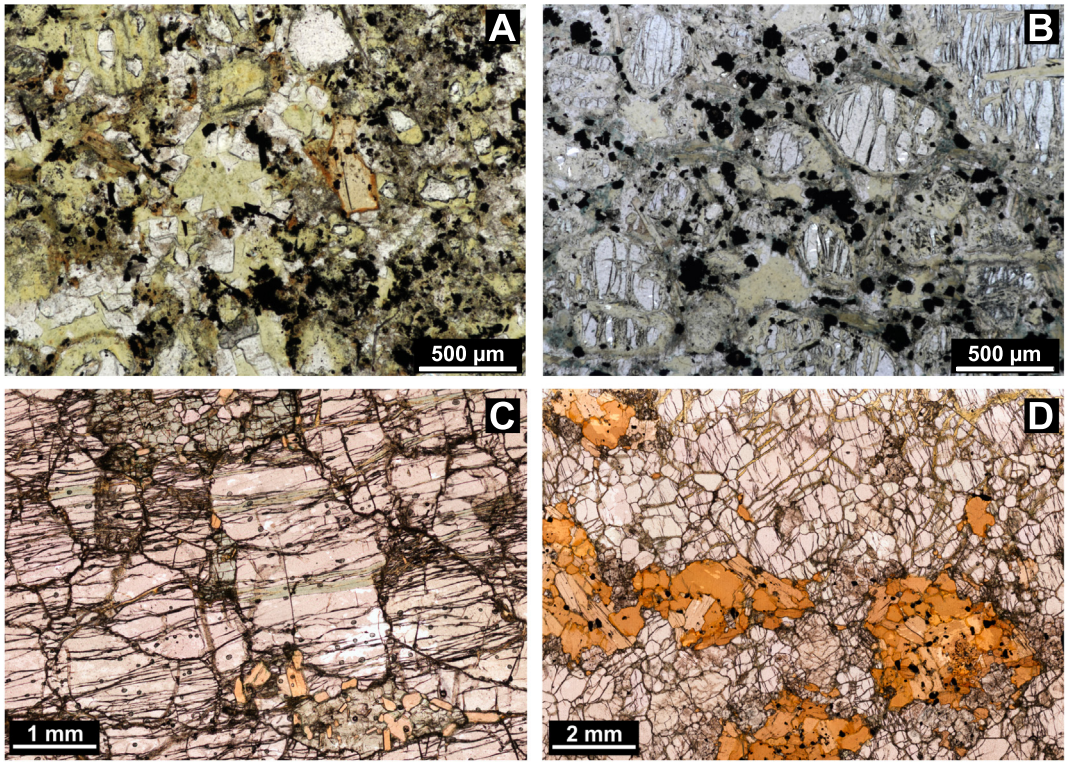

Fig. 2. Representative photomicrographs of a) kimberlite from Pyramidefjeld; b) kimberlite from Nigerdlikasik; c) phlogopite- and clinopyroxene-bearing mantle xenolith P3581-X1 from Pyramidefjeld (note the green serpentine bands forming a sub-parallel anastomosing network); d) phlogopite- and clinopyroxene-bearing mantle xenolith P3580-X1 from Nigerdlikasik. (For interpretation of the references to colour in this figure legend, the reader is referred to the web version of this article.)

subduction-related basalts (Pearce and Peate, 1995). Importantly, it is acknowledged that halogens were significant components of the Gardar mantle-derived magmas, with the peralkaline Ilímaussaq intrusion south of Pyramidefjeld in the Ketilidian Mobile Belt also displaying high halogen contents (Bailey et al., 2006). The extremely high concentrations of halogens in Gardar rocks along the southern NAC margin and the Ketilidian mobile belt have been ascribed to tapping of a subduction enriched continental lithospheric mantle domain that was probably established during the Ketilidian orogeny at ca. 1.8 Ga (Köhler et al., 2009). Metasomatism of the lithospheric mantle beneath the southern NAC margin was also concomitant with rifting during the Mesozoic shortly prior to and during the emplacement of the ca. 160–150 Ma kimberlites on the NAC preceding the splitting of the NAC with the opening of the Labrador Sea between 60 and 30 Ma (e.g. Larsen et al., 2009; Tappe et al., 2007).

3. Methods

3.1. WD-XRF

Major and trace element analyses of kimberlites from Nigerdlikasik and Pyramidefjeld (Table 1) were undertaken by X-ray fluorescence spectrometry (XRF) at Royal Holloway University of London. Analysis was undertaken using a 2010 PANalytical Axios equential X-ray fluorescence spectrometer with a 4 kW Rh-anode X-ray tube. Major elements for kimberlite samples from Nigerdlikasik and Pyramidefjeld were analyzed on fused glass discs containing a La_2O_3 heavy absorber. Trace elements were analyzed on 10 g pressed powder pellets. Fe was analyzed in both the fused glass discs and pressed pellets as a comparative internal standard. Typical reproducibility for Nd and Nb used in halogen ratios are on the order of ~1 rel % (e.g. Portnyagin et al., 2015).

3.2. Combustion ion chromatography

Simultaneous determinations of halogen (F, Cl, and Br) concentrations were undertaken at University of Tübingen by Combustion Ion Chromatography, which is an automated combination of combustion digestion (pyrohydrolysis) and ion chromatography. We used a 930 Compact IC Flex chromatograph (Metrohm) with chemical suppression and a peristaltic pump for regeneration (100 mmol/l H_2SO_4) that was connected to a combustion oven and an autosampler for solid samples (MMS 5000; Analytik Jena). For combustion, a mixture of 5–15 mg sample powder mixed with the same amount of WO_3 powder (99.995% - Aldrich 204,781) was put into a quartz vial that was capped on both sides with quartz wool and placed into glass vessels. The quartz vessels where heated in an extraction line with a constant flow of Ar (6.0; 100 ml/min) and O_2 (5.0; 300 ml/min) to 1050 °C for 12 min, followed by 10 min of post-combustion and 7 min of cooling. During combustion, a constant water flow (0.2 ml/min) was maintained. The loaded steam was collected in an absorbance module containing 4 ml of 500 ppm H_2O_2 solution. After matrix elimination (using a Metrosep A PCC 2 HC/4.0 column) the solutions were injected into the ion chromatograph. For improved detection of Br at the presence of high amounts of Cl, we used a Metrosep A Supp 5–250/4.0 (kept at 55 °C) and a Metrosep A Supp 4/5/4.0 Guard column and an eluent consisting of a mixture of 2 mmol NaOH, 1.6 mmol Na_2CO_3, and 5 vol% acetone at a flow rate of 0.7 ml/min. For quantification of the halogen and S concentrations, a primary reference solution was mixed from single element solutions (1000 mg/l; ROTH) and a quadratic 6-point-calibration curve that covered the concentrations to be quantified was assembled using the Metrohm intelligent Partial Loop Injection Technique (MiPT). The effective detection limits for powdered samples are ~10 μg/g for F and Cl, and ~ 0.3 μg/g for Br, respectively. Based on the frequent analyses of standard solutions and various reference materials (GS-N, BE-N, AGV-2; supplementary Table S1), relative uncertainties are <5–10%

Table 1
Major and trace element data of kimberlites from Majuagaa, Nigerdlikasik, Pyramidefjeld. Major element and trace element data excluding Nigerdlikasik and Pyramidefjeld and halogens from Tappe et al., (2009; 2011; 2017). Halogens with recaclc subscript are estimates of the original magma composition assuming a Cl/Nb ratio of 13.8 and a Br/Nb ratio of 0.04 (see text) and olivine contamination of ~30% (excluding samples from Tikiussaq where no contamination is present). LOI = loss on ignition. Major elements reported in wt%, trace elements reported in ppm. Total Fe reported as Fe_2O_3. *Average where multiple analyses were used, error taken as 1sd.

		Nigerdlikasik	Nigerdlikasik	Pyramidefjeld	Tikuasaaq	Tikuasaaq	Tikuasaaq	Tikuasaaq	Tikuasaaq	Tikuasaaq	Majuagaa	Majuagaa	Majuagaa	Majuagaa	Majuagaa
		P3579	P3580	P3581	488,520	488,538	488,546	488,548	488,549	488,556	MA-491702	MA-491708	MA-491712	MA-491722	MA-491741
Major	SiO_2	–	25.90	28.31	20.97	22.25	20.12	30.58	30.95	18.54	23.65	25.46	27.18	26.13	24.62
	TiO_2	–	1.80	2.60	4.43	2.86	3.74	3.70	4.02	3.56	3.10	3.33	3.85	3.77	4.01
	Al_2O_3	–	2.57	2.52	3.76	2.24	2.40	2.57	2.33	2.19	1.32	1.55	1.50	1.40	1.34
	Fe_2O_{3t}	–	10.61	13.16	15.01	13.46	14.53	13.47	14.02	14.18	10.20	11.00	12.00	11.80	11.40
	MnO	–	0.19	0.20	0.33	0.20	0.22	0.18	0.18	0.21	0.18	0.18	0.19	0.18	0.19
	MgO	–	26.80	26.41	12.87	20.25	16.45	22.29	23.79	14.76	29.51	31.59	35.02	33.59	32.98
	CaO	–	12.54	9.72	27.10	19.34	22.71	12.57	13.08	24.04	14.60	11.87	8.22	9.97	10.45
	Na_2O	–	0.09	0.24	0.15	0.12	0.11	0.17	0.14	0.10	0.12	0.10	0.10	0.08	0.11
	K_2O	–	1.40	1.10	0.92	1.12	1.14	1.41	1.44	1.02	0.21	0.30	0.28	0.13	0.06
	P_2O_5	–	0.36	0.44	0.73	1.04	0.98	0.60	0.57	1.62	0.86	0.81	0.30	0.35	0.40
	LOI	–	16.24	14.50	13.00	16.30	16.90	11.80	8.80	19.00	15.57	13.33	10.84	12.32	13.75
	Total	–	98.50	99.20	99.27	99.18	99.30	99.34	99.32	99.22	99.32	99.52	99.48	99.72	99.31
Trace	F	906	1051	1177	5399	2562	2620	2201	1320	3326	1086	1045	965	804	1131
	F_{recalc}	N/A	1366	1530	5399	2562	2620	2201	1320	3326	1629	1568	1448	1206	1697
	Cl	835	397	500	34	29	32	19	21	30	161	121	124	130	149
	Cl_{recalc}	N/A	3561	2086	4692	2001	2208	1311	1449	2070	4126	3101	2781	3332	3341
	Br	9.4	2.4	3.5	1.1	0.4	0.7	0.7	0.6	0.4	0.4	0.5	0.6	0.9	0.8
	Br_{recalc}	N/A	10	6	22	5	9	5	5	8	10	9	8	9	10
	$\delta^{37}Cl$ (‰)	+0.4	+1.1,+1.0	+0.9, + 1.4	–	–	–	–	–	–	−0.2	−0.4	−0.4	−0.5	−0.2
	$\delta^{37}Cl^*$ (‰)		+1.0 ± 0.0	+1.2 ± 0.4	–	–	–	–	–	–	–	–	–	–	–
	F/Cl	1	3	2	161	87	81	114	62	110	7	9	8	6	8
	F/Cl_{recalc}	N/A	0.4	1	1	1	1	2	1	2	0	1	1	0.4	1
	F/Nd	N/A	14	19	13	19	15	26	13	21	18	19	14	13	18
	Cl/Nb	N/A	2	4	0.1	0.2	0.2	0.2	0.2	0.2	0.7	0.7	0.8	0.7	0.8
	Br/Nb	N/A	0.01	0.03	0.002	0.003	0.003	0.006	0.005	0.002	0.002	0.003	0.004	0.005	0.004
	Br/Cl	N/A	0.006	0.007	0.03	0.01	0.02	0.04	0.03	0.01	0.003	0.004	0.005	0.007	0.005
	%Cl loss		86	69	99	99	99	99	99	99	95	95	94	95	94
	%Br loss		70	25	95	93	93	85	88	95	95	93	90	88	90

(1-sigma level) for F and Cl but up to ~20% for Br, depending on concentrations.

The crushed phlogopite aliquots from cratonic mantle xenolith samples P3580-X1 and P3581-X1 were analyzed for their halogen contents using the same methodology as for kimberlites.

3.3. IRMS $\delta^{37}Cl$ determination

Cl isotope analyses were completed at the University of Texas at Austin based on the procedures of Eggenkamp (1994) as modified by Barnes and Sharp (2006) and Sharp et al. (2007). Bulk rock powders were washed five times each in ultrapure deionized water in order to remove any potential surficial chlorine contamination, and subsequently dried. Chloride was extracted from the rock powders into an aqueous solution via pyrohydrolysis (Magenheim et al., 1994). Chloride in solution was precipitated as AgCl via reaction with $AgNO_3$. The AgCl was then reacted with CH_3I at 80 °C for 48 h to produce CH_3Cl, which is the analyte introduced into the mass spectrometer. CH_3Cl was purified from excess CH_3I on a gas chromatographic system in a continuous He flow before introduction into a ThermoElectron MAT 253 mass spectrometer. Data are reported in standard per mil notation (‰) relative to SMOC (Standard Mean Ocean Chloride; $\delta^{37}Cl$ value = 0‰). Precision is ±0.2‰ (1σ) based on the long-term average of three internal seawater standards and one internal serpentinite standard. The serpentinite rock standard demonstrates that the pyrohydrolysis process does not increase the analytical error. The phlogopite aliquot from cratonic mantle xenolith sample P3581-X1 was also analyzed for its Cl isotope composition using the same methodology as for kimberlites.

3.4. Energy-dispersive X-ray spectroscopy via scanning electron microscopy (SEM-EDX)

Chlorine contents of serpentine within peridotite xenoliths were analyzed in thin section by energy-dispersive X-ray spectroscopy via scanning electron microscopy (SEM-EDX) at the iCRAG laboratory, Trinity College Dublin. Analyses were carried out using a Tescan TIGER MIRA3 field emission SEM, equipped with two Oxford XMax^n 150 mm^2 EDS detectors. The TIGER MIRA3 instrument utilizes the Oxford Instruments AZtec X-ray microanalysis software suite. We utilized a beam current of ~3.0 nA and an accelerating voltage of 15 kV with acquisition time varied to obtain a minimum of 4,000,000 counts to insure adequate counting statistics and lower detection limits. Beam current drift was restricted by frequent analysis of pure cobalt. SEM-EDX maps of serpentine veins within peridotite xenolith P3581-X1 were imaged under the same analytical conditions, with 50 ms dwell time per pixel. Estimated sample X-ray excitation volume, calculated from the X-ray range expression of Anderson and Hasler (1966), allowed for the optimization of the spatial resolution of the map while minimizing over sampling. The instrument was calibrated using a suite of appropriate mineral standards from the Smithsonian Institute (Jarosewich, 2002; Jarosewich et al., 1980) following the method of Ubide et al. (2017). Typical analytical biases for SiO_2, MgO and FeO obtained through analysis of San Carlos olivine (NMNH111312-44) were < 0.5 wt% for SiO_2 and MgO and 1.9 wt% for FeO. For Cl analysis the instrument was calibrated using the natural scapolite (meionite) NMNH R6600 obtained from the Smithsonian Institute. Two quality control standards were used to verify accuracy; a natural reference material fluorapatite, NMNH 10402 (Jarosewich et al., 1980) and scapolite BB-1 (Kendrick, 2012; Kendrick et al., 2013). The observed analytical biases for Cl analyses were < 5%. The detection limit for chlorine utilizing this analytical setup is ~0.10 wt%. The Cl SEM-EDX maps were calibrated with spot data collected from sites (n = 10) within the same field of view from the same analytical session to provide quantitative X-ray intensities.

4. Results

Bulk rock halogen concentrations (including $\delta^{37}Cl$ values) and selected ratios of halogens and lithophile trace elements for the kimberlite samples from Majuagaa, Tikiusaaq, Pyramidefjeld, and Nigerdlikasik are reported in Table 1. Halogen concentrations of phlogopite in cratonic mantle xenoliths are reported in Table 2.

4.1. Elemental halogen compositions of Greenland kimberlites

Majuagaa kimberlite samples (n = 5) have a relatively uniform halogen concentrations of 804 to 1131 ppm F, 121 to 161 ppm Cl, and 0.4 to 0.9 ppm Br (Fig. 3). Halogen concentrations in the Tikiusaaq kimberlites (n = 6) range from 1320 to 5399 ppm F and 19 to 33 ppm Cl (Fig. 3). Tikiusaaq kimberlites are significantly more enriched in F and depleted in Cl relative to Majuagaa (Fig. 3). As a consequence, F/Cl ratios in kimberlites from Tikiusaaq range between 60 and 160 as opposed to the lower ratios of between 6 and 9 seen at Majuagaa. Bromine concentrations of Tikiusaaq kimberlites are similar to their counterpart from Majuagaa, ranging from 0.4 to 0.7 ppm.

Nigerdlikasik and Pyramidefjeld kimberlites (n = 3) have similar F concentrations to Majuagaa, ranging from 906 to 1177 ppm. However, the heavy halogens Cl and Br are significantly more enriched (Fig. 3). Chlorine contents for Nigerdlikasik and Pyramidefjeld kimberlites range from 397 to 835 ppm, and Br contents range from 2.4 to 9.4 ppm (Fig. 3). Ratios of F/Cl in kimberlites from Nigerdlikasik and Pyramidefjeld range from 1 to 3, which is lower than the F/Cl recorded in the Majuagaa and Tikiusaaq kimberlites, whereas Br/Cl ratios are similar to kimberlites samples from Majuagaa but lower than those from Tikiusaaq. The Br/Cl ratios are almost always enriched in the studied kimberlites (0.003–0.007 for Majuagaa; 0.006–0.007 for Pyramidefjeld-Nigerdlikasik; 0.01–0.04 for Tikiusaaq) compared to estimates for MORB and OIB (Fig. 3), which have Br/Cl of ~0.0028 (Kendrick et al., 2017).

Fluorine content is negatively correlated with MgO of the studied kimberlites. Ratios of F/Nd are broadly similar in all samples spanning a range from 9 to 26 (Fig. 4), comparable to those observed for both MORB and OIB (Fig. 4). Ratios of Cl/Nb are variable between the studied kimberlite locations (Fig. 4), with the lowest values observed at Tikiusaaq (0.07 to 0.2), which is up to an order of magnitude lower than for Majuagaa (0.7 to 0.8). The Cl/Nb ratios decrease with decreasing MgO content for these kimberlites and are much lower relative to MORB and OIB, which range from 3 to 51 (Kendrick et al., 2017). The highest ratios of Cl/Nb are observed for the kimberlites from Nigerdlikasik and Pyramidefjeld, which extend to between 2 and 4, close to those of MORB and OIB (Fig. 4-5). The Br/Nb ratios of kimberlites from Tikiusaaq and Majuagaa range from 0.002 to 0.006 and are elevated compared to those reported for OIB and MORB (0.009–0.137; Kendrick et al., 2017).

By contrast, Br/Nb ratios of kimberlites from Nigerdlikasik and Pyramidefjeld range between 0.01 and 0.03, closer to values reported for MORB and OIB (Kendrick et al., 2017).

4.2. Halogens in mantle-derived peridotite xenoliths

The Cl concentrations of serpentine in phlogopite bearing lherzolite and harzburgite xenoliths from hosted in kimberlites from Pyramidefjeld and Nigerdlikasik range from below the detection limit at ~0.10 wt% to 1.4 wt%, averaging 0.37 ± 0.27 wt% (1σ) (n = 60) (Table 2 and Table S2). It is apparent texturally that in some cases the serpentine veins predate kimberlite magmatism, since infiltration of relatively Cl-depleted kimberlite melt is observed within some peridotite xenoliths where randomly distributed kimberlitic veinlets crosscut the pre-existing serpentine vein network showing a preferred planar fabric (Fig. 6; non-orientated thin section). Halogen concentrations of phlogopite aliquots recovered from peridotite xenoliths from

Table 2
Average major element compositions of serpentine in mantle xenoliths from kimberlites from Nigerdlikasik and Pyramidefjeld, Greenland. Elements reported in wt%.

Locality	Pyramidefjeld		Nigerdlikasik		Nigerdlikasik		Nigerdlikasik		Nigerdlikasik		Nigerdlikasik	
ID	P3581-X1		P3579-X1		P3580-X1		P3580-X2		P3580-X3		P3580-X4	
Rock	phl-lhz		phl-harz		phl-hrz		phl-hrz		phl-lhz		phl-hrz	
analyses	n = 10	1σ	n = 10	1σ	n = 10	1σ	n = 10	1σ	n = 10	1σ	n = 10	1σ
SiO_2 (wt%)	32.66	0.65	38.14	1.73	37.03	2.12	36.22	2.30	37.07	2.27	37.39	2.30
Al_2O_3	0.19	0.03	0.27	0.09	0.23	0.06	0.19	0.10	0.27	0.09	0.09	0.03
FeO_t	7.38	0.45	7.46	2.15	7.69	1.75	5.82	1.51	6.93	1.10	6.12	1.41
MgO	37.50	0.26	35.85	2.68	36.69	2.46	36.57	1.74	35.18	2.15	37.06	2.65
NiO	0.27	0.04	0.26	0.12	0.10	0.03	0.22	0.04	0.10	0.03	0.07	0.05
Na_2O	0.16	0.01	0.17	0.02	0.20	0.01	0.21	0.05	0.20	0.02	0.20	0.01
Cl	0.81	0.28	0.25	0.07	0.34	0.17	0.38	0.25	0.23	0.18	0.35	0.17
Total	78.98		82.39		82.28		79.61		79.98		81.28	

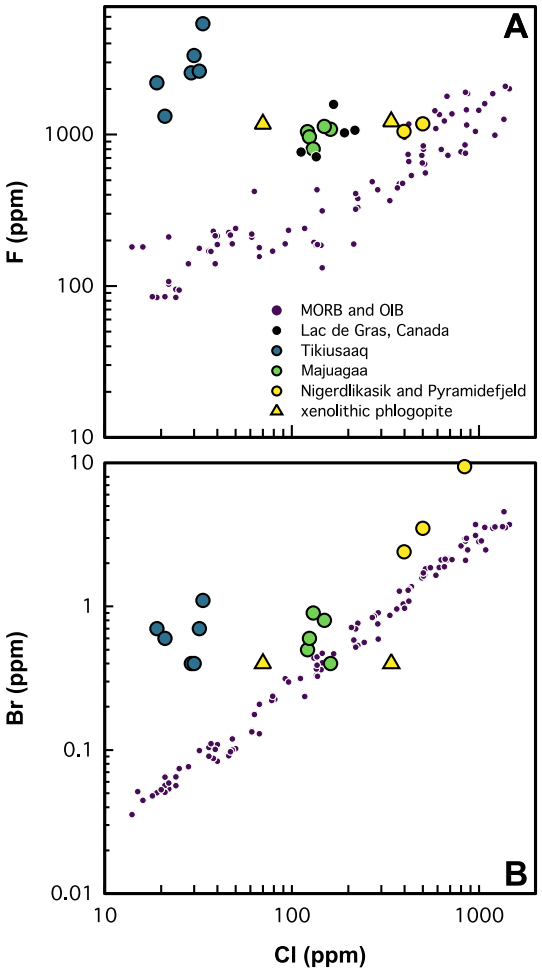

Fig. 3. F vs Cl and Br vs Cl plots (ppm) for Greenland kimberlites from Majuagaa, Tikiusaaq, Nigerdlikasik and Pyramidefjeld. Also shown are MORB and OIB compositions from the database of Kendrick et al. (2017).

Nigerdlikasik (P3580-X1) and Pyramidefjeld (P3581-X1) are 1218 and 3988 ppm F and 339 and 70 ppm Cl, respectively, at constant Br of ~0.4 ppm (Table 3).

4.3. Chlorine isotope compositions of Greenland kimberlites

Kimberlite samples from Majuagaa have negative δ^{37}Cl values ranging from −0.5 to −0.2‰ (Table 1). Chlorine isotope compositions were not analyzed for kimberlites from Tikiusaaq due to their extremely low Cl concentrations. In contrast, kimberlites from Nigerdlikasik and Pyramidefjeld have positive δ^{37}Cl values of +0.4 to +1.0‰ and + 1.2‰, respectively. The phlogopite aliquot from peridotite xenolith P3581-X1 from Nigerdlikasik yielded a δ^{37}Cl value of +1.3‰ that is analytically indistinguishable from the Cl isotopic composition of the host kimberlite.

5. Discussion

The volatile and halogen compositions of kimberlite melts are the culmination of a series of processes: melting of the convecting mantle; potential assimilation or fusion of metasomatic phases during passage through the cratonic mantle; and fractionation of the kimberlite magma during melt evolution upon further ascent. Subsequently, the halogen systematics of kimberlites may be modified by late-stage fluid exsolution, degassing, weathering and crustal contamination. Consequently, bulk kimberlite halogen contents are unlikely to reflect the primary magmatic abundances. Nonetheless, by examining ratios of halogens and lithophile incompatible trace elements of equal incompatibility during partial melting in the mantle (e.g. F/Nd; Cl/Nb; Br/Nb) it is possible to detect fingerprints left by some of these processes. The utility of these ratios is that neither Nd nor Nb are expected to be depleted by processes that lead to volatile loss in kimberlites and these two elements are hosted in relatively resistant accessory groundmass phases (e.g. Cr-spinel; ilmenite; rutile; apatite; perovskite).

5.1. Halogen behavior in magmatic systems

The overwhelming concentration of halogens in the Earth's crust and hydrosphere reflect, principally, their high incompatibilities during partial melting of the mantle and subsequent magma differentiation. However, within silicate melts the larger ionic radii of Cl and Br relative to F implies that they behave highly incompatible compared to the moderately incompatible F during partial melting processes. Experimental partitioning of F and Cl between olivine and orthopyroxene and silicate melt seems to confirm this, with F being less incompatible than Cl (Beyer et al., 2012; Joachim et al., 2014). The incompatibility contrast between F and Cl (and Br) probably results from the similar ionic radii of F^- to that of the OH^- group. Fluorine is likely incorporated similarly to OH^- in the 'nominally anhydrous minerals' olivine, orthopyroxene, clinopyroxene and garnet, which comprise the bulk of the mineralogy of the upper mantle (Beyer et al., 2012; Crépisson et al., 2014; Joachim et al., 2014). The constancy of Br/Cl ratios observed in MORB and OIB magmas suggests that Br and Cl are similarly incompatible during mantle melting (e.g. Kendrick et al., 2012a, 2017). Elements with comparative mantle incompatibility, such as F and Nd or Cl, Br and Nb, are not easily fractionated by mantle melting. Thus, their relative abundances in a mantle-derived melt can be considered

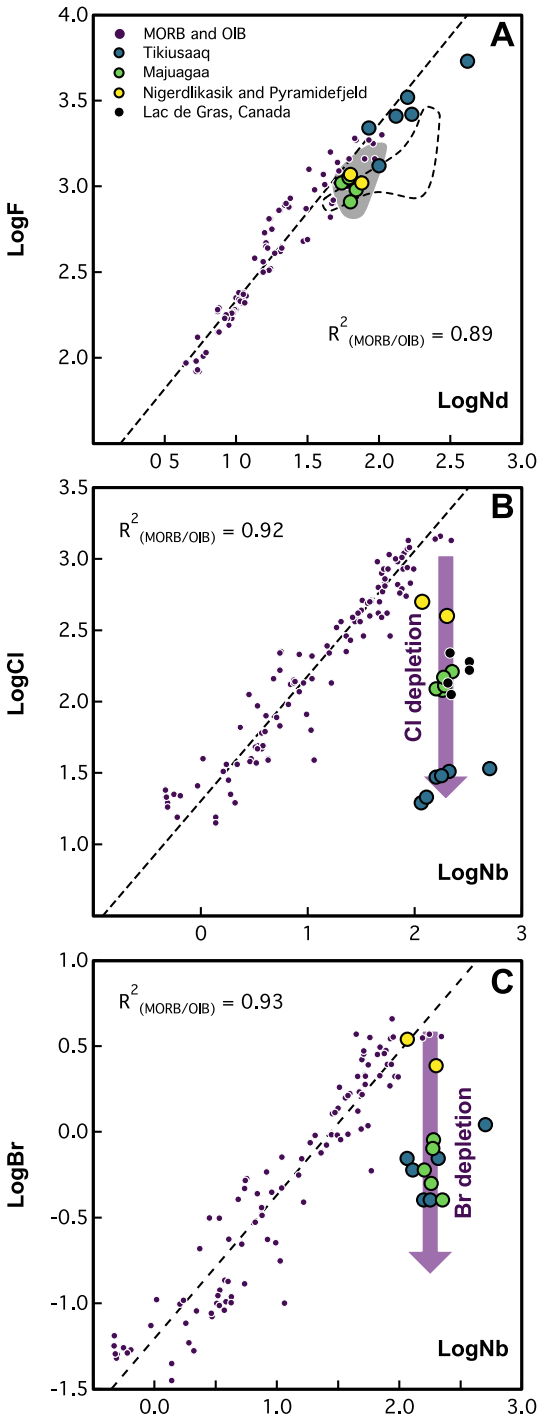

Fig. 4. Log-log plots of F, Cl and Br (ppm) against elements of similar incompatible lithophile trace elements in kimberlites from Majuagaa, Tikiusaaq Nigerdlikasik and Pyramidefjeld. Arrows show apparent Cl and Br loss. Also shown are data for MORB and OIB from the database of Kendrick et al. (2017). The grey shaded and stippled fields in Panel A show F/Nd ratios of non-crustally contaminated and crustally contaminated kimberlites from Lac de Gras in Canada, respectively. Data for Lac de Gras hypabyssal kimberlites are from Kjarsgaard et al. (2009) and Tappe et al. (2013).

representative of the source and they can be used to trace the effects of magmatic differentiation and late-stage disturbance.

Fluorine, Cl and Br also differ in how they partition between melts and magmatic fluids. Fluorine is extremely soluble in mafic silicate melts and far more soluble than H_2O at shallow crustal pressures (Webster et al., 2018). By contrast, Cl and Br partition in favor of magmatic fluids (Cadoux et al., 2018; Webster et al., 2018) suggesting that significant fractionation and loss of Cl and Br can occur during the exsolution of volatiles upon magma emplacement. Experimental data investigating the immiscibility between chloride or carbonate and silicate melt fractions show that the halogens partition into the chloride or carbonate phase (Veksler et al., 2012). This preference for halogens to partition into carbonate or chloride relative to silicate melt fractions is supported by the extreme halogen concentrations of rare carbonatite lavas (e.g. Mangler et al., 2014) and potentially by the extreme Cl concentrations observed in the Udachnaya kimberlite (Kamenetsky et al., 2007, 2014), although the origin of the Cl at this locality is highly controversial (Kopylova et al., 2016).

Halogens are the fourth (Cl) and fifth order volatiles (F) after H_2O, CO_2 and S released from present-day terrestrial volcanism via degassing (Webster et al., 2018). However, in mafic silicate systems, the closest analogue for comparison with kimberlites, F and Cl are probably retained in the melt rather than partitioning into a vapor phase. Thus, both elements are only significantly mobilized during *syn*-eruptive degassing or during the late degassing of residual magmas (Aiuppa, 2009).

5.2. Fluorine in kimberlites from the NAC

Ratios of F and Nd span a similar range to MORB and OIB (Fig. 3; 4a). As F and Nd appear to be similarly incompatible during partial melting of peridotite irrespective of source enrichment (i.e. MORB vs OIB; Kendrick et al., 2017), the F/Nd ratios of the NAC kimberlites imply that no significant F addition or loss relative to Nd has occurred during or after kimberlite magma emplacement (Fig. 4a). Constancy of F/Nd could be a general feature of kimberlites because this geochemical signature is also observed for hypabyssal kimberlites from the Lac de Gras field in Canada (Fig. 4a). The constancy of F/Nd in kimberlites, similar to MORB and OIB, is not surprising because F displays extremely high solubility in CaO-MgO rich and SiO_2-Al_2O_3 poor silicate melts (Brey et al., 2009). Furthermore, fluoride-silicate immiscibility is hard to achieve, or simply does not exist, in multicomponent systems (e.g. Dolejš, 2004; Veksler et al., 1998). Fluorine is also unlikely to be disturbed (either lost or gained) by the interaction with late-stage fluids or post-emplacement weathering, because post-emplacement remobilization of F is not observed in similar ultramafic volatile-rich rocks (carbonatites) from Oldoinyo Lengai (Mangler et al., 2014), which is probably owed to fluoride insolubility. Thus, it is reasonable to argue that F is retained in the kimberlite melt during differentiation, degassing and weathering.

Whilst F/Nd ratios are broadly constant across all measured kimberlites from the NAC, the F concentrations show some variation. Kimberlites from Majuagaa, Nigerdlikasik and Pyramidefjeld display similar contents of F of ~1000 ppm, which are similar to those recorded in kimberlites from NW Canada and southern India (Kjarsgaard et al., 2009; Paul et al., 1976). By contrast, kimberlites from Tikiusaaq are distinctly more F enriched, similar to some anomalously F-rich kimberlites from central India, which contain up to 0.75 wt% F (Paul et al., 1976).

The variable F contents of kimberlites from the NAC could derive from (1) varying degrees of partial melting of the mantle, (2) interaction with the lithospheric mantle during magma ascent, and (3) differentiation or crustal contamination. We can exclude the assimilation of F-rich metasomatized mantle within the kimberlites on account of the similarity of F/Nd ratios with those from MORB and OIB (Fig. 4a). Within the cratonic mantle, phlogopite is likely to be the major F host particularly on account of its ubiquity in mantle xenoliths from the NAC. Generally, phlogopite in the lithospheric mantle has Nd contents in the <1 ppm range (Aulbach et al., 2017; Grégoire et al., 2002, 2003), whilst F reaches wt% abundance levels (e.g. Smart et al., 2019; Smith et al., 1981). Thus, assimilation of mantle phlogopite during magma ascent would be expected to substantially increase the F/Nd of kimberlites. We also see no clear relationship between F contents and K_2O (an often-used

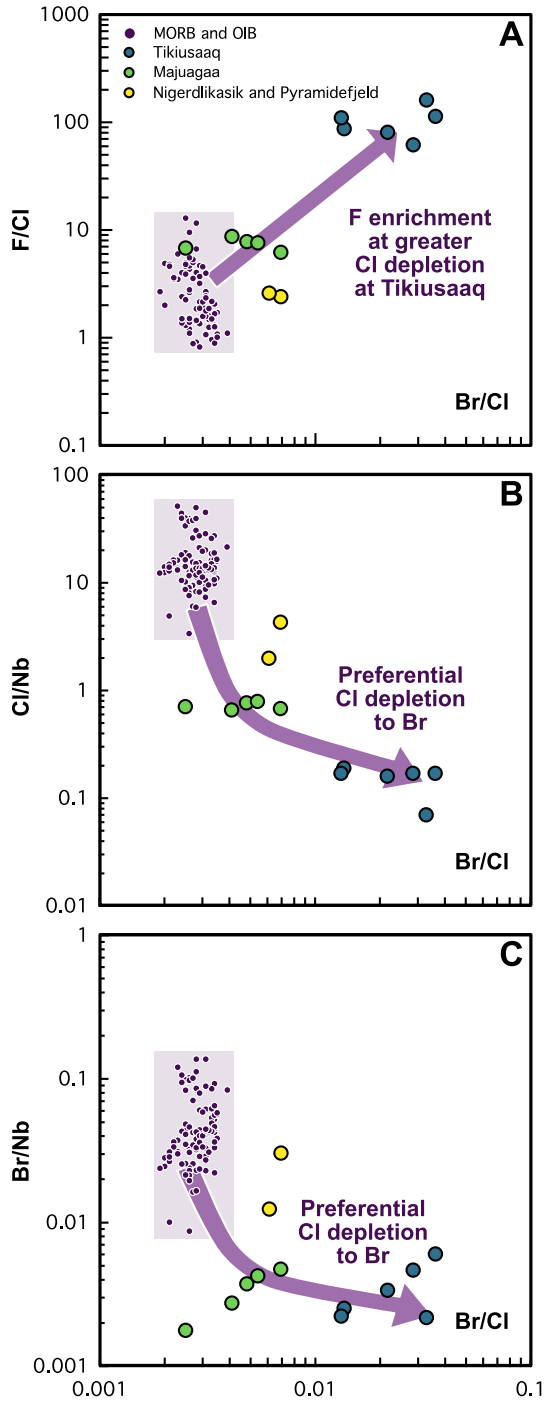

Fig. 5. Plots of halogen / lithophile trace element ratios against Br/Cl in kimberlites from Majuagaa, Tikiusaaq, Nigerdlikasik and Pyramidefjeld. Also shown are MORB and OIB data from the database of Kendrick et al. (2017).

proxy for phlogopite assimilation) in the kimberlites from Majuagaa, Nigerdlikasik and Pyramidefjeld, or Lac de Gras in Canada (Kjarsgaard et al., 2009). Surprisingly, kimberlites from Tikiusaaq display a negative correlation between F and K_2O contents. Collectively this suggests a lack of influence of mantle phlogopite on the bulk F contents of Greenland kimberlites.

For the same reason, phlogopite growth in the cratonic mantle underlying Majuagaa, Nigerdlikasik and Pyramidefjeld and removal of F from kimberlite magma as a result of the metasomatizing of the surrounding lithospheric mantle during ascent is equally unlikely, because this would be expected to lower F/Nd. Even if mica growth occurred together with clinopyroxene, as is commonly observed in mantle xenoliths from the southern NAC (e.g. Aulbach et al., 2017), typical Nd contents of clinopyroxene in phlogopite-rich xenoliths are simply not high enough (Aulbach et al., 2017; Grégoire et al., 2002, 2003) to balance F/Nd to mantle-like values. The apparent lack of influence of metasomatized lithosphere on the F budget of NAC kimberlite magmas is a surprising result, particularly for kimberlites from Nigerdlikasik and Pyramidefjeld, which contain mantle xenoliths with high modal abundances of phlogopite. However, F abundances in phlogopite are comparable to the kimberlites themselves (Tables 1 and 3), so that F addition to magmas by means of phlogopite digestion may be inconsequential to the kimberlite F budget.

Crustal contamination is unlikely to explain the high F contents at Tikiusaaq because crustally contaminated kimberlites from Canada often have disturbed and depressed F/Nd ratios (Stippled field; Fig. 4a), outside the range observed for MORB and OIB. Furthermore, none of our Greenland kimberlite samples show geochemical fingerprints of crustal contamination applying the screens devised by Kjarsgaard et al. (2009). Furthermore, the kimberlite dykes from Tikiusaaq display no disturbance of their Pb isotope compositions, an isotopic tracer that is particularly sensitive to contamination of mantle-derived melts by felsic cratonic basement rocks (Tappe et al., 2017).

A lower degree of melting at Tikiusaaq is consistent with higher F contents and could reconcile with the strong incompatible trace element enrichments compared to kimberlites from Majuagaa and Pyramidefjeld (Larsen et al., 2009; Tappe et al., 2011a, 2011b, 2017), and from key localities in southern Africa (le Roex et al., 2003; Tappe et al., 2020a).

It is also possible that F varies in kimberlites from the NAC as a function of magma differentiation. However, unlike kimberlites from Tikiusaaq, dykes from Nigerdlikasik, Majuagaa and Pyramidefjeld also contain a high contribution of xenocrystic olivine of ~30% (Nielsen and Sand, 2008; this study). The sampling of olivine with an average Mg# of ~92.8 (Bernstein et al., 2007) from the cratonic mantle displaces whole rock compositions to higher Mg# and higher SiO_2 contents than might be expected for uncontaminated magmas. Therefore, kimberlites from Tikiusaaq are unlikely to be more 'evolved' than those from Nigerdlikasik, Majuagaa and Pyramidefjeld at least in terms of magmatic differentiation. Note that the accumulation of xenocrystic olivine in kimberlite will make no change to the bulk F/Nd, because both elements are highly incompatible in olivine (Beyer et al., 2012; De Hoog et al., 2010; Joachim et al., 2014; Stead et al., 2017).

Removal of xenocrystic olivine, whilst increasing F contents by ~30%, fails to increase the F contents to the high values observed for kimberlites from Tikiusaaq. This suggests that olivine xenocryst contamination can only partly explain the higher F contents of samples from Tikiusaaq. Kimberlites from Tikiusaaq may more closely resemble near-primary melts of CO_2-fluxed peridotite (Tappe et al., 2017) than the serpentine-bearing kimberlite dykes from Nigerdlikasik, Majuagaa and Pyramidefjeld (Emeleus and Andrews, 1975; Nielsen et al., 2009). In this case, the high F concentrations of the Tikiusaaq kimberlites would be a primary melt feature similar to other low-degree ultramafic alkaline magmas such as lamproites, for which F has been shown to display the highest concentrations in the least differentiated magmas (e.g., Edgar et al., 1996). This observation is consistent with melt inclusions from the Roger kimberlite, on the Slave craton that display high F contents (Abersteiner et al., 2017).

The absence of groundmass serpentine in kimberlites from Tikiusaaq, considered to be amongst the last crystallizing phases in kimberlites irrespective of its origin, could support the view that these rocks are closer to a 'primary' kimberlite composition than those from the other studied localities on the NAC. It is unsurprising that the absence of serpentine in kimberlites from Tikiusaaq makes no difference to bulk rock F/Nd ratios because serpentine is argued to form from

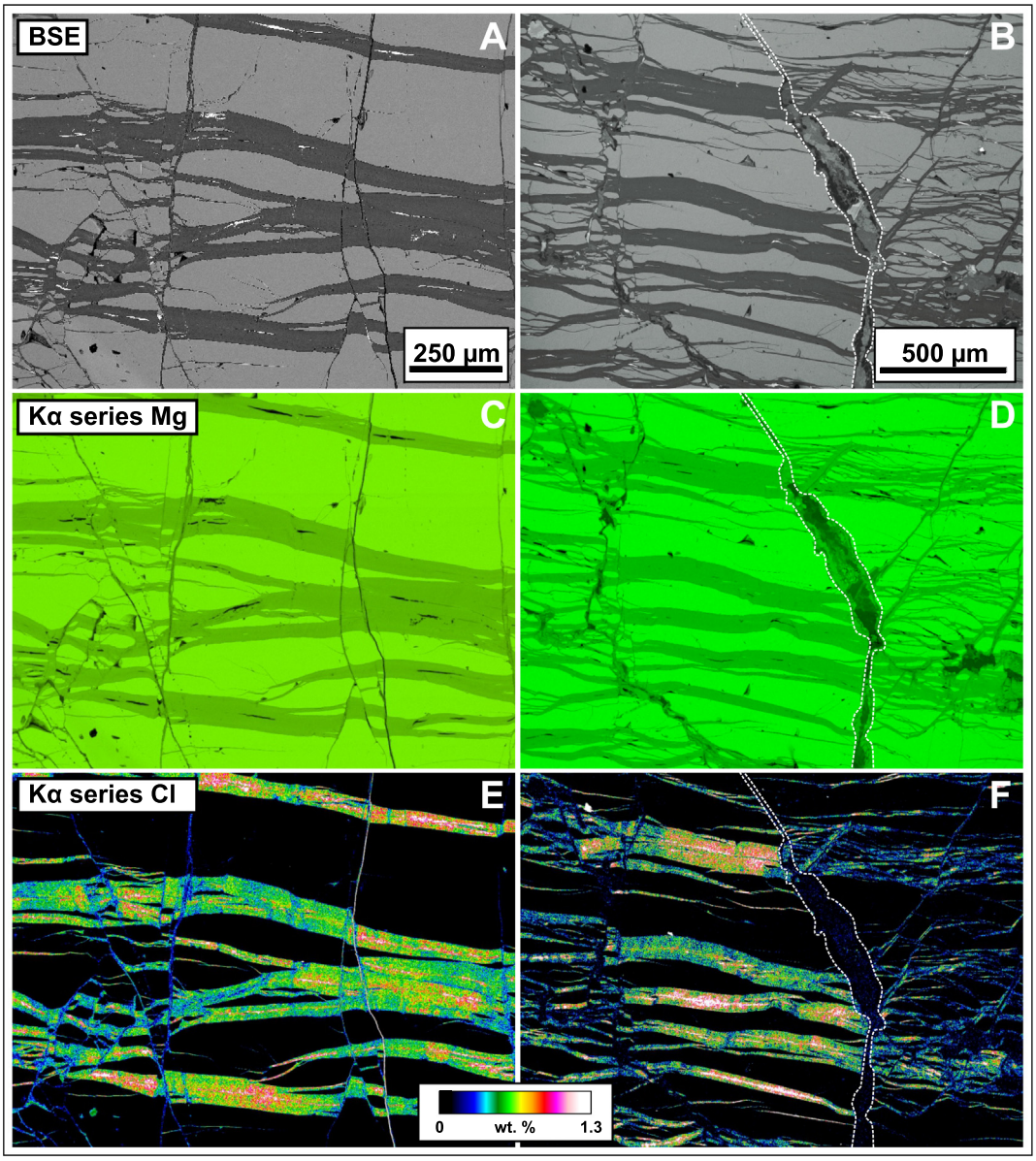

Fig. 6. SEM-EDX maps of serpentine veins in peridotite xenolith P3581-X1 from Pyramidefjeld. A and B) Backscatter electron images in two locations (note the infiltration of kimberlite along fracture in B). C and D) Kα series X-ray intensities for Mg. E and F) Kα series X-ray intensities for Cl (note the low Cl contents of the melt infiltrating the fracture seen in B and D).

late-stage fluids (Giuliani et al., 2014; Mitchell, 2008) and both F and Nd show a preference for partitioning into silicate melts rather than fluid phases (Aiuppa et al., 2009; Cullers et al., 1973). The absence of serpentine in samples from Tikiusaaq might passively increase the volume of F-bearing phases in the groundmass (e.g., phlogopite, apatite) thereby increasing the F contents of the kimberlite. On balance we suggest that the high F contents in the kimberlites from Tikiusaaq are most likely derived from their mineralogy and the lack of serpentine, but whether the higher F contents reflect less differentiated melts remains unclear. Ultimately, the overlapping F/Nd ratios of kimberlites from the NAC and modern oceanic basalts (OIB and MORB) suggest that F in all of our samples is magmatically derived.

5.3. Cl and Br in kimberlites from the NAC

5.3.1. Evidence of Cl and Br depletion

Unlike F, the Cl and Br concentrations in all studied kimberlites show significant evidence of depletion relative to what might be expected from a near-primary kimberlite melt. Chlorine, Br and Nb are thought to be similarly incompatible during melting (Kendrick et al., 2017) and both Cl/Nb and Br/Nb are commonly depleted in kimberlites from the NAC relative to MORB and OIB magmas (Fig. 5), whilst Br/Cl are mostly elevated relative to MORB and OIB (Figs. 3 and 5). Ratios of Cl/Nb are depleted relative to MORB and OIB in all

Table 3
Elemental and isotopic halogen data from phlogopite within mantle xenoliths from Nigerdlikasik and Pyramidefjeld. *Average where multiple analyses were taken, error taken as 1sd. Halogens reported in ppm.

Location	Nigerdlikasik	Pyramidefjeld
xenolith	P3580-X1	P3581-X1
F (ppm)	1218	1175
Cl	339	70
Br	0.4	0.4
F/Cl	3.6	16.8
$\delta^{37}Cl$	+1.1, +1.5	–
$\delta^{37}Cl^{*}$	+1.3 ± 0.3	–

the studied kimberlites, varying from minor depletions in kimberlites from Nigerdlikasik and Pyramidefjeld and moderate depletion at Majuagaa to strongly depleted at Tikiusaaq. Kimberlites from Nigerdlikasik and Pyramidefjeld overlap the range reported for MORB and OIB magmas in Br/Nb, with kimberlites from Majuagaa and Tikiusaaq showing greater depletion (Fig. 5). Variations in the ratios of these equally incompatible trace elements for the NAC kimberlites occur at near-constant Nb contents, which are similar to the median Nb concentration of kimberlites from key localities worldwide of ~180 ppm (Becker and Le Roex, 2006; le Roex et al., 2003; Tappe et al., 2013). Accordingly, the low Cl/Nb ratios are controlled by lower-than-expected Cl abundances than would be expected for a near primary melt. Bromine is depleted to a lesser extent than Cl in kimberlites from the NAC (Figs. 4 and 5), leading to elevated Br/Cl ratios. These ratios imply that a significant portion of magmatically derived Cl and, to a lesser extent Br, has been lost from the NAC kimberlites.

Using the measured Nb contents (116–225 ppm; and 505 ppm in 488520; Tappe et al., 2011a, 2011b, 2017) in our samples from Majuagaa and Tikiusaaq and a Cl/Nb ratio of 13.8, the median value of Cl/Nb from OIB and MORB (calculated from the database of Kendrick et al., 2017) we suggest the Cl content of the proto kimberlite melt to be between 0.20 and 0.47 wt%. These values are slightly lower than the estimated 0.61–0.72 wt% (estimated from Cl/U of 680 assuming U and Cl are similarly incompatible during mantle melting) for the Roger kimberlite on the Canadian Shield (Abersteiner et al., 2017). Using their Nb values for a direct comparison with our Cl/Nb ratios gives similar estimated Cl contents of between 0.60 and 0.75 wt% for the Roger kimberlite. We estimate that kimberlites from Majuagaa and Tikiusaaq have lost at least ~94–99% of their original Cl contents. For Br, using a Br/Nb ratio of 0.04, the median value of Br/Nb in MORB and OIB (also calculated from the database of Kendrick et al., 2017), we suggest the Br content of the primary kimberlite to be 5–9 ppm and a loss of ~88–95% of its original inventory. By contrast, kimberlites from Pyramidefjeld and Nigerdlikasik appear less Cl and Br depleted compared to those from Tikiusaaq and Majuagaa with depletions of 69% and 86% for Cl and only 25% and 70% for Br.

Substantial Cl loss from the kimberlites is consistent with the observed F/Cl ratios of the kimberlites which are either similar to, or significantly higher than seen in MORB or OIB (Fig. 5). This is the opposite of what one might expect since F is expected to be less incompatible during mantle melting than Cl and since kimberlites form from some of the smallest degrees of melting it should be expected that they would have low F/Cl ratios. However, reconstructed F/Cl ratios using recalculated Cl contents based on Cl/Nb ratios are indeed substantially lower, typically below the MORB values (Table 1).

Depletion levels of 88–99% observed at Majuagaa and Tikiusaaq are similar to the extremely low and unsupported Na_2O contents of our samples and kimberlites worldwide, which is inconsistent with melting of fertile mantle peridotite (Stamm and Schmidt, 2017). Melting experiments of fertile peridotite at 7 GPa suggest that kimberlite melts should have far higher Na_2O contents of between 2.4 and 5.6 wt% at 7 GPa (Stamm and Schmidt, 2017) compared to the <0.2 wt% abundance common to kimberlites worldwide (Kjarsgaard et al., 2009; Tappe et al., 2017). The mismatch between experimental data and that of kimberlites worldwide suggests a depletion of between 83 and 97% of their Na_2O contents. As with Na_2O, significant CO_2 depletion is observed in hypabyssal kimberlites suggesting up to 20 wt% loss during magma emplacement (e.g. Dongre and Tappe, 2019). We suggest that Cl and Br depletion in kimberlites from the NAC broadly follows the trend of other soluble elements in kimberlites globally. Shortly after or during magma emplacement near the Earth's surface (at 2 to 5 km paleodepths), the kimberlite dykes from the NAC experienced preferential removal of the heavy halogens during late-stage processes in the order of Cl > Br, with potentially up to 99% of their original Cl and Br inventories lost during post-emplacement processes.

5.3.2. Possible causes for Cl and Br depletions in kimberlites

Evidence of higher than measured Cl contents in, and thus halogen loss from, primitive kimberlite magmas is suggested by secondary melt inclusions within minerals (e.g. olivine, Cr-spinel, monticellite and apatite) in kimberlites which display a variety of halogen-bearing carbonates, phosphates as well as halite/sylvite (Abersteiner et al., 2017, 2019b). Groundmassdjerfisherite in kimberlite and their hosted mantle xenoliths (Abersteiner et al., 2019a; Clarke et al., 1994) amongst other water soluble halogen-bearing phases (Parthasarathy et al., 2002; Watkinson and Chao, 1973), including those from Udachnaya (e.g. Kamenetsky et al., 2004, 2014), further supports the notion that an early-stage kimberlite magma is initially more Cl-rich. The most commonly advocated mechanisms for the recognized volatile (e.g., CO_2, alkalis, halogens) loss in kimberlites are as follows:

(i) Exsolution of volatiles either as a result of immiscibility/filter pressing of carbonate (i.e. carbonatite) melts (Kamenetsky and Yaxley, 2015; Tappe et al., 2020b) or chloride phase and silicate melts (e.g. Kamenetsky et al., 2007, 2014).
(ii) Degassing of kimberlite magmas close to the Earth's surface (Brooker et al., 2011).
(iii) Interactions with deuteric (i.e. magmatically-derived) fluids and/or influx of groundwater into the kimberlite (Giuliani et al., 2014; Mitchell, 2008).

5.3.2.1. Exsolution of volatiles as a result of liquid immiscibility?. The temporal and spatial relationship of kimberlites and related rocks including carbonatites is widely acknowledged (Dalton and Presnall, 1998; Tappe et al., 2020b; Woolley and Kjarsgaard, 2008), with the coexistence of kimberlite and carbonatite intrusives commonly (but not exclusively) explained by exsolution and removal of a substantial fluid/carbonate phase during kimberlite magma ascent through the shallow cratonic mantle and crust (Tappe et al., 2017). The enriched halogen compositions of carbonatite magmas (Mangler et al., 2014) suggest that the exsolution of a carbonate melt phase via liquid immiscibility from a carbonated silicate magma could offer a solution to the extreme Cl and Br depletion observed in kimberlites from the NAC, especially because kimberlites and carbonatites are frequently observed to coexist in West Greenland (Larsen and Rex, 1992; Tappe et al., 2009, 2011a, 2011b, 2012). However, for Nigerdlikasik and Pyramidefjeld in South-West Greenland there are no coincident carbonatites or extremely carbonate-rich melts exposed that could be conjugate to kimberlite magmas (Larsen et al., 2009). The apparent absence of carbonatites at this location excludes a straightforward link between Cl and Br depletion as a result of carbonate-silicate immiscibility. In any case, it is becoming clear with an increasing body of evidence that simple genetic relationships between kimberlites and carbonatites through increasing degrees of differentiation are not always tenable (Tappe et al., 2020a), and that silicate-dominated and carbonate-rich magmas often accompany one another rather than being always strictly associated (Gittins and Harmer, 2003).

On the other hand, chloride immiscibility could explain the extreme Cl depletion of the Greenland kimberlites, and this mechanism has been invoked to explain the extreme Cl and Na_2O enrichments of the rather unique Udachnaya-East kimberlite (Kamenetsky et al., 2007, 2014). Regardless of whether the halogen composition of the Udachnaya-East kimberlite is a primary magmatic feature or reflects crustal contamination by evaporites (c.f. Kopylova et al., 2013, 2016; Kamenetsky et al., 2014), this case at last demonstrates that chloride immiscibility can occur in kimberlite melts. Halide segregations are extremely sensitive to post-emplacement alteration either in response to weathering or the influx of late stage deuteric or meteoric fluids (see Section 5.3.2.3). Loss of halogens and Na_2O during progressive weathering is documented for natrocarbonatite lavas from Oldoinyo Lengai (Mangler et al., 2014; Zaitsev and Keller, 2006) and has been invoked to explain

the mismatch between the halogen contents of melt inclusions and bulk kimberlite from Udachnaya-East (e.g. Abersteiner et al., 2017; Kamenetsky et al., 2009).

5.3.2.2. Degassing. Modeling suggests that Cl and Br degassing in mafic systems is likely to occur at relatively shallow depths during near-surface *syn*-eruptive degassing, with Cl and Br fairly reticent to partitioning into a vapor phase (e.g.Aiuppa, 2009; Cadoux et al., 2018). It is apparent from melting experiments on synthetic kimberlite that a substantial CO_2 vapor phase is expected to be released at similarly shallow levels of <3 km within the Earth's upper crust (Moussallam et al., 2015). It is conceivable that halogens could be present in such a vapor phase, and – contrary to earlier assumptions (e.g., Mitchell, 2008) - recent modeling studies show that hypabyssal kimberlites have undergone significant CO_2-degassing (Dongre and Tappe, 2019). Nonetheless, the fairly restricted range in HCl/HF and HCl/HBr ratios measured in present-day volcanic gases from a given tectonic setting suggests that significant fractionation does not occur during degassing (Aiuppa, 2009; Cadoux et al., 2018). Thus, it appears unlikely that degassing of kimberlite magmas during emplacement can explain the here observed halogen fractionation.

5.3.2.3. Interaction with or loss of fluids during kimberlite magma emplacement. The origin of H_2O in kimberlites is strongly debated and is suggested to be either deuteric (i.e. magmatic; e.g. Mitchell, 2008, 2013), meteoric, or some mixture of the two sources (e.g. Giuliani et al., 2014; Sparks et al., 2009). Both Cl and Br are extremely fluid mobile and suspected primary halogen hosting phases in kimberlites are water-soluble. Therefore, deuteric and meteoric fluids may provide a conduit for the post-emplacement remobilization of halogens and their loss from kimberlite into the surrounding country rocks. Direct evidence of Cl mobilization by fluids in kimberlites is shown by the high abundances and heterogeneous distribution of Cl in serpentine from kimberlites at various localities, including from the Maniitsoq field (Kamenetsky et al., 2009). These authors showed that the earliest generation of serpentine, replacing olivine macrocrysts, displays the highest Cl contents, whilst later serpentine generations are relatively depleted in Cl. This suggests that the Cl content of the fluid was at its peak at the beginning of replacement and subsequently decreased with further influx of meteoric H_2O-rich fluids. Similar evidence is seen in samples from Nigerdlikasik and Pyramidefjeld, where the earliest serpentine in olivine of mantle-derived xenoliths shows extreme Cl enrichments, while serpentine in late-stage cross-cutting veins contains significantly less Cl (Fig. 6).

Kimberlites from Tikiusaaq are more depleted in Cl than from Majuagaa, Nigerdlikasik, Pyramidefjeld and Lac de Gras, with the key difference between these samples the absence of serpentine in kimberlites from Tikiusaaq. Serpentine is enriched in Cl other tectonic settings (e.g. Kodolányi et al., 2012), and the absence of serpentine could explain the depleted Cl in kimberlites from Tikiusaaq. The lack of serpentine may reflect a lack of late-stage fluid interaction suggesting that the relative abundance of halogens in the Tikiusaaq kimberlites may resemble the primary kimberlite magma composition. However, this is hard to reconcile with the lower Cl contents of Tikiusaaq kimberlites, because melt/fluid inclusion evidence from kimberlites worldwide advocates higher Cl contents of near-primary kimberlite melts (Abersteiner et al., 2017, 2019a; Kamenetsky et al., 2009). Alternatively, the absence of serpentine in the crystallizing assemblage at Tikiusaaq may have driven Cl-loss by forcing a large amount of the initial Cl into the residual melt, from where it either exsolved or precipitated as water-soluble halogen-rich phases, subsequently lost during weak post-emplacement alteration or sample preparation.

Late-stage fluid movement in kimberlite magmas during emplacement offers significant potential to disturb and deplete their halogen inventories, with the extent of remobilization most likely depending on the abundance of soluble halogen-bearing phases and serpentine within the primary phase assemblage.

5.3.2.4. Variability amongst Greenland kimberlites. Whilst it is beyond the scope of this study to speculate on the origins of H_2O in kimberlite, clearly the subject is important as to whether halogens are magmatically derived and how the potential influx of external fluids affects the distribution of Cl and Br in kimberlites.

We suggest that variable Cl (and to a lesser extent Br) depletion in NAC kimberlites is the result of partitioning of the heavy halogens from the hybrid kimberlite magma into exsolving carbonate melt or chloride fluid, with some potential for removal of Cl-Br-bearing minerals during weathering, with variable roles of these processes at the locations studied. Chlorine loss is most extreme in Tikiusaaq kimberlites, which we attribute to the absence of serpentine. We infer that the absence of serpentine in kimberlites from Tikiusaaq results in the concentration of F and Cl in the residual melt which could be more susceptible to Cl loss via exsolution and/or weathering.

Whilst significant Cl depletion also occurred at Majuagaa via exsolution and/or weathering, the occurrence of groundmass serpentine may have allowed a greater proportion of the original Cl inventory to be retained. An alternative explanation for the high Br/Cl ratios of the Tikiusaaq and Majuagaa kimberlites is that the observed Cl depletion is a primary magmatic feature with possible implications for the halogen contents of the mantle source. High Br/Cl ratios are observed in olivine hosted melt inclusions from the Emperor Seamount chain, where they are attributed to the involvement of subducted oceanic crust in the mantle source to these lavas (Broadley et al., 2019).

By contrast, kimberlites from Nigerdlikasik and Pyramidefjeld show only moderate heavy halogen depletion, suggesting that exsolution or weathering may have been less extreme. An alternative explanation for the elevated Cl and Br contents and lower Br/Cl ratios of kimberlites from Nigerdlikasik and Pyramidefjeld is that they sample a distinct halogen enriched mantle reservoir not sourced in kimberlites from Majuagaa and Tikiusaaq. This possibility is explored below.

5.3.3. Heavy halogen enrichment in kimberlites from South-West Greenland

Kimberlite samples from Majuagaa with lower Cl and high Br/Cl have δ^{37}Cl values ranging from −0.5 to −0.2‰ overlapping those values recorded for depleted upper mantle as sampled by MORB (-0.2 ± 0.5‰, $n = 12$; Sharp et al., 2007, 2013) (Fig. 7). Similar δ^{37}Cl values have also been obtained for halite from the Udachnaya-East kimberlite (0.0 ± 0.25‰, $n = 3$; Sharp et al., 2007) and from variably altered carbonatites (-0.15 ± 0.4‰, $n = 8$; Eggenkamp and Van Groos, 1997). Therefore, the δ^{37}Cl values observed for kimberlites from Majuagaa are consistent with Cl being sourced from the convecting upper mantle (Fig. 7), in agreement with their Sr-Nd-Hf isotopic compositions that are reminiscent of a moderately depleted upper mantle source (Tappe et al., 2011a, 2011b).

By contrast, the ca. 150 Ma kimberlites from Nigerdlikasik and Pyramidefjeld are less depleted in Cl, display lower Br/Cl ratios, and have positive δ^{37}Cl values of +0.4 to +1.2‰, which are too heavy for depleted upper mantle values. This suggests sampling of a distinctly different halogen reservoir compared to that seen in samples from Majuagaa farther north on the NAC. Significant fractionation of chlorine isotopes occurs only at relatively low temperatures (e.g. Balan et al., 2019; Schauble et al., 2003) by processes either close to or at the Earth's surface. Therefore, Cl isotope fractionation may have occurred during volatile exsolution, magmatic degassing or interaction with magmatic and meteoric fluids (Barnes and Sharp, 2017). Degassing of Cl in mafic systems is generally controlled by release of HCl vapor and this is likely minimal as MORB basalts show extremely limited isotope variability close to 0‰ (Sharp et al., 2007, 2013), whilst carbonatite lavas - thought to undergo degassing - are remarkably similar to MORB. The limited data of the effect of post-emplacement alteration in ultramafic magmas

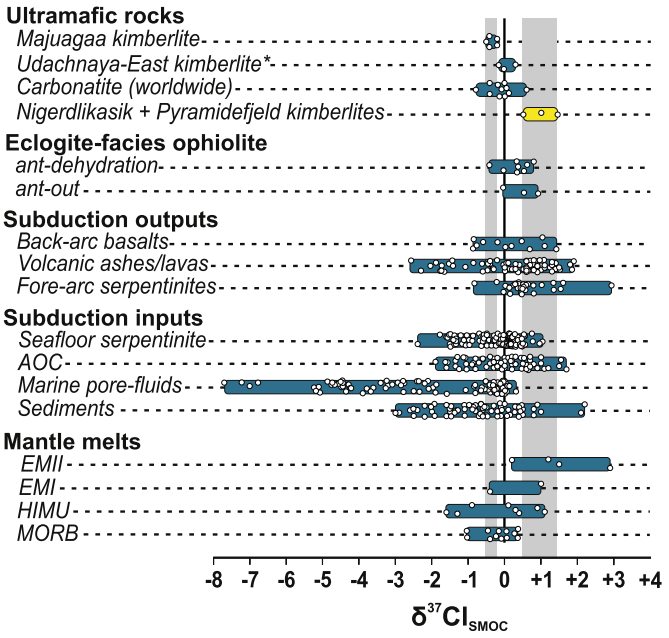

Fig. 7. The $\delta^{37}Cl$ ‰ [versus standard mean ocean chloride (SMOC)] compositions of Greenland kimberlites from Majuagaa, Nigerdlikasik and Pyramidefjeld. The compilation of published $\delta^{37}Cl$ values for mantle-derived melts from the ocean basins (MORB: mid-ocean ridge basalt; HIMU 'high-μ': defined as mantle domains with highly radiogenic $^{206}Pb/^{204}Pb$ compositions; EM-I: enriched-mantle I; EM-II: enriched-mantle II), subduction inputs and outputs, and eclogite-facies ophiolites is from Barnes and Sharp (2017, and references therein). Carbonatite data and kimberlite data from Udachnaya-East (Eggenkamp and Van Groos, 1997; Sharp et al., 2007). *Kimberlite data is taken from analyses of halite rather than whole-rock analysis. The grey bars serve as visual aid to highlight the newly acquired data from Greenland.

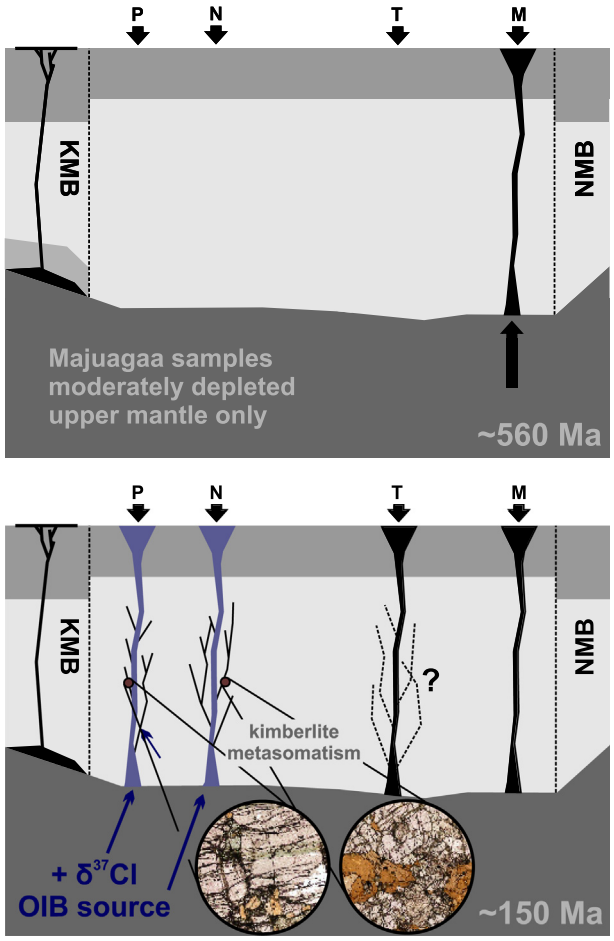

Fig. 8. Schematic displaying the scenario in which recycled halogens are sampled from an OIB-type reservoir in the convecting upper mantle by 150 Ma old kimberlite magmatism along the southern NAC margin. P = Pyramidefjeld, N = Nigerdlikasik, T = Tikiusaaq, M = Majuagaa. KMB = Ketilidian mobile belt, NMB = Nagsuqtoqidian mobile belt.

are from the carbonatite study of Eggenkamp and Van Groos (1997), for which all but one analyses yielded negative $\delta^{37}Cl$ values, suggests that post-emplacement alteration has only a minor effect on the chlorine isotope compositions in ultramafic volatile-rich rocks. We reiterate that all of our studied kimberlite samples, including those from Nigerdlikasik and Pyramidefjeld, are free of sub-aerial alteration and that serpentine, where present, formed probably during the magmatic stage.

Therefore, we argue that positive $\delta^{37}Cl$ values observed in kimberlites from Nigerdlikasik and Pyramidefjeld are unlikely to derive from near-surface chlorine isotope fractionation. This inference is supported by the similar $\delta^{37}Cl$ composition of phlogopite from mantle xenolith P3580-X1, which likely formed within the cratonic mantle at mid-lithospheric depth (Aulbach et al., 2017). Collectively, this suggests that the positive $\delta^{37}Cl$ values of kimberlites from the southern margin of the NAC reflect the original magma composition. The positive $\delta^{37}Cl$ values of kimberlites from Nigerdlikasik and Pyramidefjeld overlap a range of subduction zone inputs within the oceanic lithosphere (e.g., altered oceanic crust, serpentinite, sediments) and are also similar to values for subduction zone products (Fig. 7). On this basis it appears permissible that the kimberlite magmas from the southern NAC margin sampled a mantle reservoir that contains recycled halogens.

5.4. Possible origins of high $\delta^{37}Cl$ in kimberlites from the NAC margin

Due to the hybrid nature of kimberlite magmas the recycled halogen reservoir and positively fractionated $\delta^{37}Cl$ values sampled at Nigerdlikasik and Pyramidefjeld could derive from either:

i. recycled lithosphere components within the convecting mantle source of kimberlites (Fig. 8); or
ii. interaction of asthenosphere-derived proto-kimberlite melts with halogen-enriched cratonic mantle lithosphere (Fig. 9).

The first scenario may imply that there was a temporal halogen enrichment beneath the NAC, because the ca. 560 Ma kimberlite from Majuagaa shows no such evidence for recycled Cl in their convecting upper mantle source (Fig. 7). The second possibility suggests a heterogeneous spatial distribution of recycled halogens within the NAC mantle lithosphere, where the kimberlite magmas at the southern craton margin assimilated abundant recycled halogens upon ascent whilst those from the craton interior digested mainly refractory components of the Archean mantle lithosphere.

5.4.1. Scenario-1: Sampling of a positive $\delta^{37}Cl$ component in the convecting mantle

The positive $\delta^{37}Cl$ values recorded for samples from Nigerdlikasik and Pyramidefjeld suggest that the kimberlite magmas may have sampled an OIB-type reservoir in the convecting mantle. Although sampling of an EM-type reservoir is consistent with the higher Cl and Br contents of the ca. 150 Ma kimberlites from the southern craton margin (see supplementary data of Kendrick et al., 2017), their Sr-Nd-Hf-Pb isotopic compositions do not support magma origins from EM-type reservoirs in the convecting mantle (Tappe, unpublished data), but rather point to a depleted convecting mantle source that has experienced moderate levels of re-enrichment, similar to the isotopic signature of the coeval Tikiusaaq kimberlites in the craton interior (Tappe et al., 2012, 2017). The Sr–Nd isotope data for metasomatically introduced clinopyroxene

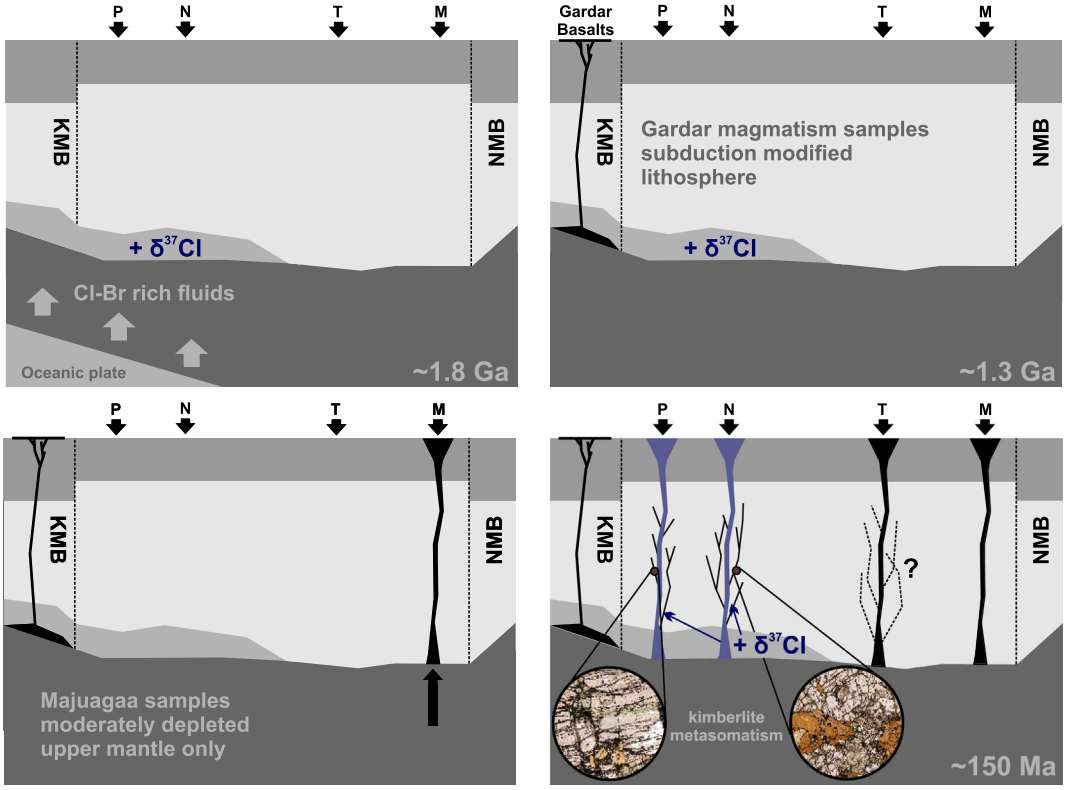

Fig. 9. Schematic displaying the scenario in which recycled halogens are derived from a subduction-modified lithospheric mantle reservoir with the main phase of metasomatism at 1.8 Ga during the adjacent Ketilidian orogeny (KMB). These metasomes influenced Gardar rift magmatism at 1.3 Ga and kimberlite magmatism at 150 Ma. Kimberlite-induced metasomatism manifests as enrichments of the cratonic lithosphere with new generations of phlogopite and clinopyroxene (see Aulbach et al., 2017).

in mantle-derived peridotite xenoliths from the southern NAC margin reveal similar moderately depleted convecting mantle sources for the metasomatic agents that were probably linked to the 150 Ma kimberlite magmatism (Aulbach et al., 2017).

These radiogenic isotope systematics render any straightforward mix between an EM-type reservoir and the depleted MORB mantle impossible. Consequently, the positive δ^{37}Cl compositions of kimberlites from the southern craton margin require most likely a halogen-enriched lithospheric mantle source that imparted heavy Cl isotope signatures to passing kimberlite melts sourced from the moderately depleted convecting mantle beneath the NAC.

Olivine-hosted melt inclusions from Pyramidefjeld record $^{3}He/^{4}He$ values between 4.6 and 9.7 Ra (Tachibana et al., 2006), which is similar to MORB values (8 ± 2 Ra; Graham, 2002). Although Tachibana and co-workers also proposed a high $^{3}He/^{4}He$ signature of these kimberlites from Greenland, the presence of primordial components in ultradeep isolated mantle sources to kimberlite magmatism has recently been challenged on the basis of a comprehensive ^{182}W isotope survey (Tappe et al., 2020b).

An ancient recycled oceanic crust component is often advocated to explain the anomalous decoupled Nd–Hf isotopic compositions of kimberlites worldwide (e.g. Nowell et al., 2004; Tappe et al., 2020b). Such material could potentially explain the positive δ^{37}Cl values of kimberlites from Nigerdlikasik and Pyramidefjeld, but it is doubtful whether significant volumes of Cl and Br can enter all the way into the deep upper mantle sources of kimberlites past the 'subduction factory' (Weiss et al., 2015).

5.4.2. Scenario-2: Sampling of an enriched δ^{37}Cl component in the cratonic mantle

Whilst the shallow lithospheric mantle of the NAC is known to be extremely refractory (Bernstein et al., 2007), it has not escaped the effects of metasomatism, particularly along the southern margin (Aulbach et al., 2017, 2019; Tappe et al., 2017; van Acken et al., 2017; Wittig et al., 2010). Major metasomatic events appear to coincide with the Ketilidian orogeny at ca. 1.8 Ga (Aulbach et al., 2017; Wittig et al., 2010) and with rifting during the Mesoproterozoic and Mesozoic (Larsen et al., 2009; Tappe et al., 2007, 2017).

It is possible that metasomatism of the southern NAC margin occurred during ca. 1.8 Ga northward-directed subduction of oceanic lithosphere under the ancient continent (Chadwick and Garde, 1996; Garde et al., 2002). In this scenario halogen-rich fluids could have been liberated from the subducting oceanic lithosphere and acted as metasomatic agents within the overriding continental lithosphere. The potential for halogen enrichment of the deep cratonic lithosphere and its diamond endowment is well documented (Burgess et al., 2002, 2009; Hecker et al., 2020; Johnson et al., 2000; Smith et al., 1981; Weiss et al., 2015) and has been linked to subduction-derived halogens (Weiss et al., 2015; Broadley et al., 2016, 2018). It is possible that the lithosphere underlying the southern NAC margin is similarly enriched in halogens and that this halogen reservoir was scavenged by asthenosphere-derived small-volume kimberlite melts during their ascent at ca. 150 Ma (Fig. 9). Indeed, the extreme halogen-rich compositions of the ca. 1.3 Ga Gardar mantle-derived magmas, including the large peralkaline Ilímausaaq intrusion of the nearby Ketilidian Mobile Belt, have been attributed to tapping of subduction enriched continental lithospheric mantle domains that may have been established during the Ketilidian orogeny at ca. 1.8 Ga (Köhler et al., 2009).

The presence of subduction-enriched lithosphere along the southern NAC margin is consistent with the enriched δ^{37}Cl values of phlogopite from a mantle xenolith recovered from the Nigerdlikasik kimberlite. However, the metasomatic nature of most mantle-derived xenoliths from the southern NAC margin has been attributed to the introduction of low-degree volatile-rich melts from the asthenosphere during Mesozoic rifting of the NAC rather than to Proterozoic metasomatic events (Aulbach et al., 2017).

Nonetheless, metasomatism by fluids derived from dehydration of subducted serpentinized lithosphere could offer a solution. Generally, fluids released during serpentine dehydration are enriched in heavy halogens and display positive δ^{37}Cl values (Fig. 7). Provided that serpentine is an extremely poor repository of lithophile trace elements in raw abundance terms (e.g. Kodolányi et al., 2012; Kodolányi and Pettke, 2011), metasomatic agents sourced from subducted serpentinites may introduce copious amounts of volatiles, including Cl and Br, into the cratonic mantle lithosphere while leaving the lithophile trace element budgets largely unaffected. Therefore, the absence of enriched $^{87}Sr/^{86}Sr$ compositions in mantle xenoliths from Pyramidefjeld (Aulbach et al., 2017) may not provide conclusive evidence against a Proterozoic subduction-related metasomatic event during which fluids were sourced from dehydrating oceanic slabs. Indeed, Late Gardar (ca. ~1.3 Ga) basaltic magmatism formed from large-scale decompression melting from an enriched continental mantle share geochemical similarities with subduction zone basalts yet display no enriched $^{87}Sr/^{86}Sr$ compositions (Goodenough et al., 2002). As subduction metasomatism was most likely to have occurred during the Ketilidian orogeny, it is possible that ancient halogen enriched metasomes might not impart enriched $^{87}Sr/^{86}Sr$ compositions when sampled in subsequent magmatism.

We prefer assimilation of subduction-enriched cratonic mantle as the source of the heavy halogen enrichment and positive δ^{37}Cl signature of kimberlites from the southern NAC margin, because this model reconciles best with the regional variability of halogen geochemical signatures and the geologic evolution of the NAC and surrounding mobile belts. Such a scenario implies that the cratonic mantle lithosphere can represent a long-term repository of recycled halogens. However, it cannot be excluded that the halogen geochemical signature of Greenland kimberlites originated from the convecting mantle – a controversy that requires further work in the near future.

6. Conclusions

The combination of elemental and isotopic halogen analyses of fresh magmatic kimberlites and entrained mantle-derived peridotite xenoliths offers a powerful tool to trace volatile loss from kimberlites and detect recycled volatiles within their mantle sources. Our main findings are as follows:

1. Fluorine in kimberlite appears to be controlled by melting in the convecting upper mantle evidenced by F/Nd ratios that overlap those of MORB and OIB.
2. Unlike F, both Cl and Br (albeit to a lesser degree) undergo significant loss of up to 99% during kimberlite magma emplacement in the crust and post-emplacement processes, as evidenced by depleted Cl/Nb and Br/Nb ratios.
3. Whilst all kimberlites studied here broadly follow the above pattern, there exists some variability in their halogen systematics. Kimberlites from Tikiusaaq are significantly enriched in F but show the largest depletion in Cl compared to other kimberlites for which such data are available. We attribute this geochemical signature to the groundmass mineralogy of the studied Tikiusaaq kimberlites, which are almost serpentine-free. We suggest that the absence of serpentine passively increases the proportion of F-bearing phases such as phlogopite and apatite. It is possible that Cl-depletion is a primary feature of kimberlite magmas and a hallmark of less differentiated magmas, although this idea remains unclear.
4. By contrast, kimberlites from the southern NAC margin display a relative enrichment of Cl and Br, and they have a positive δ^{37}Cl signature, which is indicative of recycled halogens in their mantle source. We suggest that the 'enriched' halogen signature of kimberlites from Nigerdlikasik was derived by assimilation of metasomatized mantle lithosphere, where the enriching agents had been sourced from subducting oceanic lithosphere. However, our dataset cannot exclude the alternative possibility that the positive δ^{37}Cl signature originated in an OIB-type source within the convecting mantle.

Regardless of the ultimate origin of the recycled δ^{37}Cl values observed at Nigerdlikasik and Pyramidefjeld, this study reveals spatial variability in the halogen compositions of kimberlites and highlights the possibility that the lithospheric mantle might represent a long-term halogen repository.

Declaration of Competing Interest

The authors declare that they have no known competing financial interests or personal relationships that could have appeared to influence the work reported in this paper.

Acknowledgements

Mathew Thirlwall is thanked for collecting WD-XRF data. This research was funded by SFI grant 15/ERC/B3131 to ET. BCH acknowledges support from a Government of Ireland postgraduate scholarship from the Irish Research Council held by BCH (GOIPG/2017/1132). The TCD iCRAG laboratory is supported by SFI grant SFI/RI/3227. ST acknowledges support by the DSI-NRF CIMERA Centre of Excellence at the University of Johannesburg, South Africa. JDB was partially supported by NSF grant EAR-1850749. The authors have no competing interests to declare. We thank Sonja Aulbach, Sally Gibson and an anonymous reviewer for their detailed and constructive reviews, which helped us to better balance our arguments and Maya Kopylova for the editorial handling of this submission.

Appendix A. Supplementary data

Supplementary data to this article can be found online at https://doi.org/10.1016/j.lithos.2021.105976.

References

Abersteiner, A., Kamenetsky, V.S., Kamenetsky, M., Goemann, K., Ehrig, K., Rodemann, T., 2017. Significance of halogens (F, Cl) in kimberlite melts: Insights from mineralogy and melt inclusions in the Roger pipe (Ekati, Canada). Chem. Geol., 0–1 https://doi.org/10.1016/j.chemgeo.2017.06.008.

Abersteiner, A., Kamenetsky, V.S., Goemann, K., Golovin, A.V., Sharygin, I.S., Giuliani, A., Rodemann, T., Spetsius, Z.V., Kamenetsky, M., 2019a. Djerfisherite in kimberlites and their xenoliths: implications for kimberlite melt evolution. Contrib. Mineral. Petrol. 174, 1–22. https://doi.org/10.1007/s00410-018-1540-8.

Abersteiner, A., Kamenetsky, V.S., Goemann, K., Golovin, A.V., Sharygin, I.S., Pearson, D.G., Kamenetsky, M., Gornova, M.A., 2019b. Polymineralic inclusions in kimberlite-hosted megacrysts: Implications for kimberlite melt evolution. Lithos https://doi.org/10.1016/j.lithos.2019.04.004.

Aiuppa, A., 2009. Degassing of halogens from basaltic volcanism: Insights from volcanic gas observations. Chem. Geol. 263, 99–109. https://doi.org/10.1016/j.chemgeo.2008.08.022.

Aiuppa, A., Baker, D.R., Webster, J.D., 2009. Halogens in volcanic systems. Chem. Geol. 263, 1–18. https://doi.org/10.1016/j.chemgeo.2008.10.005.

Anderson, C.A., Hasler, M.F., 1966. Extension of Electron Microprobe Techniques to Biochemistry by Use of Long Wavelength X-Rays, *in* Proceedings of the Fourth International Conference on X-Ray Optics and Microanalysis.

Andrews, J.R., Emeleus, C.H., 1971. Preliminary account of kimberlite intrusions from the Frederikshtb district, South-West Greenland: Rapp. Grznlands Geol. Unders. 31, 1–28.

Aulbach, S., Griffin, W.L., Pearson, N.J., O'Reilly, S.Y., 2013. Nature and timing of metasomatism in the stratified mantle lithosphere beneath the central Slave craton (Canada). Chem. Geol. 352, 153–169. https://doi.org/10.1016/j.chemgeo.2013.05.037.

Aulbach, S., Sun, J., Tappe, S., Höfer, H.E., Gerdes, A., 2017. Volatile-rich metasomatism in the cratonic mantle beneath SW Greenland: link to kimberlites and mid-lithospheric discontinuities. J. Petrol. 58, 2311–2338. https://doi.org/10.1093/petrology/egy009.

Aulbach, S., Sun, J., Tappe, S., Gerdes, A., 2019. Effects of multi-stage rifting and metasomatism on HSE- 187 Os/ 188 Os systematics of the cratonic mantle beneath SW Greenland. Contrib. Mineral. Petrol. 174, 0. https://doi.org/10.1007/s00410-019-1549-7.

Bailey, J.C., Sørensen, H., Andersen, T., Kogarko, L.N., Rose-Hansen, J., 2006. On the origin of microrhythmic layering in arfvedsonite lujavrite from the Ilímaussaq alkaline complex, South Greenland. Lithos 91, 301–318. https://doi.org/10.1016/j.lithos.2006.03.022.

Balan, E., Créon, L., Sanloup, C., Aléon, J., Blanchard, M., Paulatto, L., Bureau, H., 2019. First-principles modeling of chlorine isotope fractionation between chloride-bearing

molecules and minerals. Chem. Geol. 525, 424–434. https://doi.org/10.1016/j.chemgeo.2019.07.032.
Barnes, J.D., Sharp, Z.D., 2006. A chlorine isotope study of DSDP/ODP serpentinized ultramafic rocks: Insights into the serpentinization process. Chem. Geol. 228, 246–265. https://doi.org/10.1016/j.chemgeo.2005.10.011.
Barnes, J.D., Sharp, Z.D., 2017. Chlorine Isotope Geochemistry. Rev. Mineral. Geochem. 82. https://doi.org/10.2138/rmg.2017.82.9.
Bartels, A., Nielsen, T.F.D., Lee, S.R., Upton, B.G.J., 2015. Petrological and geochemical characteristics of Mesoproterozoic dyke swarms in the Gardar Province, South Greenland: evidence for a major sub-continental lithospheric mantle component in the generation of the magmas. Mineral. Mag. 79, 909–939. https://doi.org/10.1180/minmag.2015.079.4.04.
Becker, M., Le Roex, A.P., 2006. Geochemistry of south African on- and off-craton, group I and group II kimberlites: Petrogenesis and source region evolution. J. Petrol. 47, 673–703. https://doi.org/10.1093/petrology/egi089.
Bell, D.R., Grégoire, M., Grove, T.L., Chatterjee, N., Carlson, R.W., Buseck, P.R., 2005. Silica and volatile-element metasomatism of Archean mantle: a xenolith-scale example from the Kaapvaal Craton. Contrib. Mineral. Petrol. 150, 251–267. https://doi.org/10.1007/s00410-005-0673-8.
Bernstein, S., Kelemen, P.B., Hanghøj, K., 2007. Consistent olivine Mg# in cratonic mantle reflects Archean mantle melting to the exhauston of orthopyroxene. Geology 35, 459–462. https://doi.org/10.1130/G23336A.1.
Beyer, C., Klemme, S., Wiedenbeck, M., Stracke, A., Vollmer, C., 2012. Fluorine in nominally fluorine-free mantle minerals: Experimental partitioning of F between olivine, orthopyroxene and silicate melts with implications for magmatic processes. Earth Planet. Sci. Lett. 337–338, 1–9. https://doi.org/10.1016/j.epsl.2012.05.003.
Brey, G.P., Bulatov, V.K., Girnis, A.V., Lahaye, Y., 2008. Experimental melting of carbonated peridotite at 6-10 GPa. J. Petrol. 49, 797–821. https://doi.org/10.1093/petrology/egn002.
Brey, G.P., Bulatov, V.K., Girnis, A.V., 2009. Influence of water and fluorine on melting of carbonated peridotite at 6 and 10 GPa. Lithos 112, 249–259. https://doi.org/10.1016/j.lithos.2009.04.037.
Bridgwater, D., 1970. A compilation of K/Ar age determi- nations on rocks from Greenland carried out in 1969: Rapp. Grenlands Geol. Unders. 47–55.
Broadley, M.W., Ballentine, C.J., Chavrit, D., Dallai, L., Burgess, R., 2016. Sedimentary halogens and noble gases within Western Antarctic xenoliths: Implications of extensive volatile recycling to the sub continental lithospheric mantle. Geochim. Cosmochim. Acta 176, 139–156. https://doi.org/10.1016/j.gca.2015.12.013.
Broadley, M.W., Barry, P.H., Ballentine, C.J., Taylor, L.A., Burgess, R., 2018. End-Permian extinction amplified by plume-induced release of recycled lithospheric volatiles. Nature Geoscience 11(9), 682–687.
Broadley, M.W., Sumino, H., Graham, D.W., Burgess, R., Ballentine, C.J., 2019. Recycled components in mantle plumes deduced from variations in halogens (Cl, Br, and I), trace elements, and 3 He/ 4 He along the hawaiian-emperor Seamount Chain. Geochem. Geophys. Geosyst. 20, 277–294. https://doi.org/10.1029/2018GC007959.
Brooker, R.A., Sparks, R.S.J., Kavanagh, J.L., Field, M., 2011. The volatile content of hypabyssal kimberlite magmas: some constraints from experiments on natural rock compositions. Bull. Volcanol. 73, 959–981. https://doi.org/10.1007/s00445-011-0523-7.
Burgess, R., Layzelle, E., Turner, G., Harris, J.W., 2002. Constraints on the age and halogen composition of mantle fluids in Siberian coated diamonds. Earth Planet. Sci. Lett. 197, 193–203. https://doi.org/10.1016/S0012-821X(02)00480-6.
Burgess, R., Cartigny, P., Harrison, D., Hobson, E., Harris, J., 2009. Volatile composition of microinclusions in diamonds from the Panda kimberlite, Canada: Implications for chemical and isotopic heterogeneity in the mantle. Geochim. Cosmochim. Acta 73, 1779–1794. https://doi.org/10.1016/j.gca.2008.12.025.
Bussweiler, Y., Foley, S.F., Prelević, D., Jacob, D.E., 2015. The olivine macrocryst problem: New insights from minor and trace element compositions of olivine from Lac de Gras kimberlites, Canada. Lithos 220–223, 238–252. https://doi.org/10.1016/j.lithos.2015.02.016.
Cadoux, A., Iacono-Marziano, G., Scaillet, B., Aiuppa, A., Mather, T.A., Pyle, D.M., Deloule, E., Gennaro, E., Paonita, A., 2018. The role of melt composition on aqueous fluid vs. silicate melt partitioning of bromine in magmas. Earth Planet. Sci. Lett. 498, 450–463. https://doi.org/10.1016/j.epsl.2018.06.038.
Chadwick, B., Garde, A.A., 1996. Palaeoproterozoic Oblique Plate Convergence in South Greenland: A Reappraisal of the Ketilidian Orogen: Precambrian Crustal Evolution in the North Atlantic Region. , pp. 179–196. https://doi.org/10.1144/GSL.SP.1996.112.01.10.
Chalapathi Rao, N.V., Creaser, R.A., Lehmann, B., Panwar, B.K., 2013. Re-Os isotope study of Indian kimberlites and lamproites: Implications for mantle source regions and cratonic evolution. Chem. Geol. 353, 36–47. https://doi.org/10.1016/j.chemgeo.2012.12.013.
Clarke, D.B., Mitchell, R.H., Chapman, C.A.T., Mackay, R.M., 1994. Occurrence and origin of djerfisherite from the Elwin Bay kimberlite, Somerset Island, Northwest Territories. Can. Mineral. 32, 815–823.
Crépisson, C., et al., 2014. Clumped fluoride-hydroxyl defects in forsterite: Implications for the upper-mantle. Earth Planet. Sci. Lett. 390, 287–295. https://doi.org/10.1016/j.epsl.2014.01.020.
Cullers, R.L., Medaris, L.G., Haskin, L.A., 1973. Experimental studies of the distribution of rare earths as trace elements among silicate minerals and liquids and water. Geochim. Cosmochim. Acta 37, 1499–1512. https://doi.org/10.1016/0016-7037(73)90086-0.
Dalton, J.A., Presnall, D.G., 1998. The continuum of primary carbonatitic-kimberlitic melt compositions in equilibrium with lherzolite: Data from the system CaO-MgO-Al2O3-SiO2-CO2 at 6 GPa. J. Petrol. 39, 1953–1964. https://doi.org/10.1093/petroj/39.11-12.1953.
Dawson, J.B., Hawthorne, J.B., 1973. Magmatic sedimentation and carbonatitic differentiation in kimberlite sills at Benfontein, South Africa. J. Geol. Soc. Lond. 129, 61–85. https://doi.org/10.1144/gsjgs.129.1.0061.
Dalton, H., Giuliani, A., O'Brien, H., Phillips, D., Hergt, J., 2020. The role of lithospheric heterogeneity on the composition of kimberlite magmas from a single field: The case of Kaavi-Kuopio, Finland. Lithos 354, 105333.
De Hoog, J.C.M., Gall, L., Cornell, D.H., 2010. Trace-element geochemistry of mantle olivine and application to mantle petrogenesis and geothermobarometry. Chem. Geol. 270, 196–215. https://doi.org/10.1016/j.chemgeo.2009.11.017.
Dolejš, D., 2004. Evidence for Fluoride Melts in Earth ' s Mantle Formed by Liquid Immiscibility: Comment and Reply COMMENT. Geology: Forum, pp. 76–77. https://doi.org/10.1130/G20328.1.Mukerji.
Dongre, A., Tappe, S., 2019. Kimberlite and carbonatite dykes within the Premier diatreme root (Cullinan Diamond Mine, South Africa): New insights to mineralogical-genetic classifications and magma CO2 degassing. Lithos 338–339, 155–173. https://doi.org/10.1016/j.lithos.2019.04.020.
Edgar, A.D., Pizzolato, L.A., Sheen, J., 1996. Fluorine in igneous rocks and minerals with emphasis on ultrapotassic mafic and ultramafic magmas and their mantle source regions. Mineral. Mag. 60, 243–257. https://doi.org/10.1180/minmag.1996.060.399.01.
Eggenkamp, H.G.M., 1994. The Geochemisty of Chlorine Isotopes. Universiteit Utrecht, p. 151.
Eggenkamp, H.G.M., Van Groos, A.F.K., 1997. Chlorine stable isotopes in carbonatites: evidence for isotopic heterogeneity in the mantle. Chem. Geol. 140, 137–143.
Emeleus, C.H., Andrews, J.R., 1975. Mineralogy and petrology of kimberlite dyke and sheet intrusions and included peridotite xenoliths from South-West Greenland. Phys. Chem. Earth 9, 179–197. https://doi.org/10.1016/0079-1946(75)90016-6.
Foley, S.F., Yaxley, G.M., Kjarsgaard, B.A., 2019. Kimberlites from source to surface: insights from experiments. Elements 15, 393–398. https://doi.org/10.2138/gselements.15.6.393.
Garde, A.A., Hamilton, M.A., Chadwick, B., Grocott, J., McCaffrey, K.J.W., 2002. The Ketilidian orogen of South Greenland: geochronology, tectonics, magmatism, and fore-arc accretion during Palaeoproterozoic oblique convergence. Can. J. Earth Sci. 39, 765–793. https://doi.org/10.1139/E02-026.
Gittins, J., Harmer, R.E., 2003. An International Journal of Myth and reality in the carbonatite - silicate rock "association" Carbonatites occur commonly, but by no means universally, in the company of a wide variety of feldspathoidal igneous rocks and pyroxenites. and the term « c. pp. 19–26.
Giuliani, A., Phillips, D., Kamenetsky, V.S., Fiorentini, M.L., Farquhar, J., Kendrick, M.A., 2014. Stable isotope (C, O, S) compositions of volatile-rich minerals in kimberlites: a review. Chem. Geol. 374–375, 61–83. https://doi.org/10.1016/j.chemgeo.2014.03.003.
Giuliani, A., Graham Pearson, D., Soltys, A., Dalton, H., Phillips, D., Foley, S.F., Lim, E., Goemann, K., Griffin, W.L., Mitchell, R.H., 2020. Kimberlite genesis from a common carbonate-rich primary melt modified by lithospheric mantle assimilation. Sci. Adv. 6, 1–10. https://doi.org/10.1126/sciadv.aaz0424.
Goodenough, K.M., Upton, B.G.J., Ellam, R.M., 2002. Long-term memory of subduction processes in the lithospheric mantle: evidence from the geochemistry of basic dykes in the Gardar Province of South Greenland. J. Geol. Soc. Lond. 159, 705–714. https://doi.org/10.1144/0016-764901-154.
Graham, D.W., 2002. Noble gas isotope geochemistry of mid-ocean ridge and ocean island basalts: Characterization of mantle source reservoirs. Rev. Mineral. Geochem. 47. https://doi.org/10.2138/rmg.2002.47.8.
Grégoire, M., Bell, D., Le Roex, A., 2002. Trace element geochemistry of phlogopite-rich mafic mantle xenoliths: their classification and their relationship to phlogopite-bearing peridotites and kimberlites revisited. Contrib. Mineral. Petrol. 142, 603–625. https://doi.org/10.1007/s00410-001-0315-8.
Grégoire, M., Bell, D.R., Le Roex, A., 2003. Garnet Lherzolites from the Kaapvaal Craton (South Africa): trace element evidence for a metasomatic history. J. Petrol. 44, 629–657. https://doi.org/10.1093/petrology/44.4.629.
Halldórsson, S.A., Barnes, J.D., Stefánsson, A., Hilton, D.R., Hauri, E.H., Marshall, E.W., 2016. Subducted lithosphere controls halogen enrichments in the Iceland mantle plume source. Geology 44, 679–682. https://doi.org/10.1130/G37924.1.
Hansen, K., 1980. Lamprophyres and carbonatitic lamprophyres related to rifting in the Labrador Sea. Lithos 13, 145–152. https://doi.org/10.1016/0024-4937(80)90015-8.
Hecker, J.G., Marks, M.A.W., Wenzel, T., Markl, G., 2020. Halogens in amphibole and mica from mantle xenoliths: Implications for the halogen distribution and halogen budget of the metasomatized continental lithosphere. Am. Mineral. 105, 781–794. https://doi.org/10.2138/am-2020-7174.
Irvine, G.J., Pearson, D.G., Kjarsgaard, B.A., Carlson, R.W., Kopylova, M.G., Dreibus, G., 2003. A Re–Os isotope and PGE study of kimberlite-derived peridotite xenoliths from Somerset Island and a comparison to the Slave and Kaapvaal cratons. Lithos 71, 461–488. https://doi.org/10.1016/S0024-4937(03)00126-9.
Jarosewich, E., 2002. Smithsonian Microbeam Standards. J. Res. Nat. Inst. Stand. Technol. 107, 681. https://doi.org/10.6028/jres.107.054.
Jarosewich, E., Nelen, J. a, Norberg, J., 1980. Reference samples for electron microprobe analysis. Geostand. Newslett. 4, 43–47.
Joachim, B., Pawley, A., Lyon, I.C., Marquardt, K., Henkel, T., Clay, P.L., Ruzié, L., Burgess, R., Ballentine, C.J., 2014. Experimental partitioning of F and Cl between olivine, orthopyroxene and silicate melt at Earth's mantle conditions. Chem. Geol. 416, 65–78. https://doi.org/10.1016/j.chemgeo.2015.08.012.
John, T., Layne, G.D., Haase, K.M., Barnes, J.D., 2010. Chlorine isotope evidence for crustal recycling into the Earth's mantle. Earth Planet. Sci. Lett. 298, 175–182. https://doi.org/10.1016/j.epsl.2010.07.039.
Johnson, L.H., Burgess, R., Turner, G., Milledge, H.J., Harris, J.W., 2000. Noble gas and halogen geochemistry of mantle fluids: Comparison of African and Canadian diamonds.

Geochim. Cosmochim. Acta 64, 717–732. https://doi.org/10.1016/S0016-7037(99)00336-1.
Kamenetsky, V.S., Yaxley, G.M., 2015. Carbonate-silicate liquid immiscibility in the mantle propels kimberlite magma ascent. Geochim. Cosmochim. Acta 158, 48–56. https://doi.org/10.1016/j.gca.2015.03.004.
Kamenetsky, M.B., Sobolev, A.V., Kamenetsky, V.S., Maas, R., Danyushevsky, L.V., Thomas, R., Pokhilenko, N.P., Sobolev, N.V., 2004. Kimberlite melts rich in alkali chlorides and carbonates: a potent metasomatic agent in the mantle. Geology 32, 845–848. https://doi.org/10.1130/G20821.1.
Kamenetsky, V.S., Kamenetsky, M.B., Sharygin, V.V., Faure, K., Golovin, A.V., 2007. Chloride and carbonate immiscible liquids at the closure of the kimberlite magma evolution (Udachnaya-East kimberlite, Siberia). Chem. Geol. 237, 384–400. https://doi.org/10.1016/j.chemgeo.2006.07.010.
Kamenetsky, V.S., Kamenetsky, M.B., Sobolev, A.V., Golovin, A.V., Demouchy, S., Faure, K., Sharygin, V.V., Kuzmin, D.V., 2008. Olivine in the Udachnaya-East kimberlite (Yakutia, Russia): Types, compositions and origins. J. Petrol. 49, 823–839. https://doi.org/10.1093/petrology/egm033.
Kamenetsky, V.S., Kamenetsky, M.B., Weiss, Y., Navon, O., Nielsen, T.F.D., Mernagh, T.P., 2009. How unique is the Udachnaya-East kimberlite? Comparison with kimberlites from the Slave Craton (Canada) and SW Greenland. Lithos 112, 334–346. https://doi.org/10.1016/j.lithos.2009.03.032.
Kamenetsky, V.S., Golovin, A.V., Maas, R., Giuliani, A., Kamenetsky, M.B., Weiss, Y., 2014. Towards a new model for kimberlite petrogenesis: evidence from unaltered kimberlites and mantle minerals. Earth Sci. Rev. 139, 145–167. https://doi.org/10.1016/j.earscirev.2014.09.004.
Kendrick, M.A., 2012. High precision Cl, Br and I determinations in mineral standards using the noble gas method. Chem. Geol. 292–293, 116–126. https://doi.org/10.1016/j.chemgeo.2011.11.021.
Kendrick, M.A., Kamenetsky, V.S., Phillips, D., Honda, M., 2012a. Halogen systematics (Cl, Br, I) in Mid-Ocean Ridge Basalts: a Macquarie Island case study. Geochim. Cosmochim. Acta 81, 82–93. https://doi.org/10.1016/j.gca.2011.12.004.
Kendrick, M.A., Woodhead, J.D., Kamenetsky, V.S., 2012b. Tracking halogens through the subduction cycle. Geology 40, 1075–1078. https://doi.org/10.1130/G33265.1.
Kendrick, M.A., Arculus, R., Burnard, P., Honda, M., 2013. Quantifying brine assimilation by submarine magmas: examples from the Gal??Pagos Spreading Centre and Lau Basin. Geochim. Cosmochim. Acta 123, 150–165. https://doi.org/10.1016/j.gca.2013.09.012.
Kendrick, M.A., Hémond, C., Kamenetsky, V.S., Danyushevsky, L., Devey, C.W., Rodemann, T., Jackson, M.G., Perfit, M.R., 2017. Seawater cycled throughout Earth's mantle in partially serpentinized lithosphere. Nat. Geosci. 10. https://doi.org/10.1038/ngeo2902.
Kjarsgaard, B.A., Pearson, D.G., Tappe, S., Nowell, G.M., Dowall, D.P., 2009. Geochemistry of hypabyssal kimberlites from Lac de Gras, Canada: Comparisons to a global database and applications to the parent magma problem. Lithos 112, 236–248. https://doi.org/10.1016/j.lithos.2009.06.001.
Kodolányi, J., Pettke, T., 2011. Loss of trace elements from serpentinites during fluid-assisted transformation of chrysotile to antigorite - an example from Guatemala. Chem. Geol. 284, 351–362. https://doi.org/10.1016/j.chemgeo.2011.03.016.
Kodolányi, J., Pettke, T., Spandler, C., Kamber, B.S., Ling, K.G., 2012. Geochemistry of ocean floor and fore-arc serpentinites: Constraints on the ultramafic input to subduction zones. J. Petrol. 53, 235–270. https://doi.org/10.1093/petrology/egr058.
Köhler, J., Schönenberger, J., Upton, B., Markl, G., 2009. Halogen and trace-element chemistry in the Gardar Province, South Greenland: Subduction-related mantle metasomatism and fluid exsolution from alkalic melts. Lithos 113, 731–747. https://doi.org/10.1016/j.lithos.2009.07.004.
Kopylova, M.G., Kostrovitsky, S.I., Egorov, K.N., 2013. Salts in southern Yakutian kimberlites and the problem of primary alkali kimberlite melts. Earth Sci. Rev. 119, 1–16. https://doi.org/10.1016/j.earscirev.2013.01.007.
Kopylova, M.G., Gaudet, M., Kostrovitsky, S.I., Polozov, A.G., Yakovlev, D.A., 2016. Origin of salts and alkali carbonates in the Udachnaya East kimberlite: Insights from petrography of kimberlite phases and their carbonate and evaporite xenoliths. J. Volcanol. Geotherm. Res. 327, 116–134. https://doi.org/10.1016/j.jvolgeores.2016.07.003.
Larsen, L.M., Rex, D.C., 1992. A review of the 2500 Ma span of alkaline-ultramafic, potassic and carbonatitic magmatism in West Greenland. Lithos 28, 367–402. https://doi.org/10.1016/0024-4937(92)90015-Q.
Larsen, L.M., Heaman, L.M., Creaser, R.a., Duncan, R.a., Frei, R., Hutchison, M., 2009. Tectonomagmatic events during stretching and basin formation in the Labrador Sea and the Davis Strait: evidence from age and composition of Mesozoic to Palaeogene dyke swarms in West Greenland. J. Geol. Soc. Lond. 166, 999–1012. https://doi.org/10.1144/0016-76492009-038.
le Roex, A.P., 1986. Geochemical correlation between Southern African kimberlites and South Atlantic hotspots. Nature 324, 243–245. https://doi.org/10.1038/324243a0.
le Roex, A.P., Class, C., 2016. Metasomatic enrichment of Proterozoic mantle south of the Kaapvaal Craton, South Africa: origin of sinusoidal REE patterns in clinopyroxene and garnet. Contrib. Mineral. Petrol. 171, 1–24. https://doi.org/10.1007/s00410-015-1222-8.
le Roex, A.P., Bell, D.R., Davis, P., 2003. Petrogenesis of group I kimberlites from Kimberley, South Africa: evidence from bulk-rock geochemistry. J. Petrol. 44, 2261–2286. https://doi.org/10.1093/petrology/egg077.
Magenheim, A.J., Spivack, A.J., Volpe, C., Ransom, B., 1994. Precise determination of stable chlorine isotopic-ratios in low-concentration natural samples. Geochim. Cosmochim. Acta 58, 3117–3121.
Mangler, M.F., Marks, M.A.W., Zaitzev, A.N., Eby, G.N., Markl, G., 2014. Halogens (f, cl and br) at oldoinyo lengai volcano (Tanzania): Effects of magmatic differentiation, silicate-natrocarbonatite melt separation and surface alteration of natrocarbonatite. Chem. Geol. 365, 43–53. https://doi.org/10.1016/j.chemgeo.2013.11.027.
Mitchell, R.H., 1986. Kimberlites: Mineralogy, Geochemistry, and Petrology: New York. Plenum Press, p. 442.
Mitchell, R.H., 2008. Petrology of hypabyssal kimberlites: Relevance to primary magma compositions. J. Volcanol. Geotherm. Res. 174, 1–8. https://doi.org/10.1016/j.jvolgeores.2007.12.024.
Mitchell, R.H., 2013. Paragenesis and Oxygen Isotopic Studies of Serpentine in Kimberlite. pp. 1–12.
Moussallam, Y., Morizet, Y., Massuyeau, M., Laumonier, M., Gaillard, F., 2015. CO2 solubility in kimberlite melts. Chem. Geol. 418, 198–205. https://doi.org/10.1016/j.chemgeo.2014.11.017.
Nielsen, T.F.D., Sand, K.K., 2008. The Majuagaa kimberlite dike, Maniitsoq region, West Greenland: Constraints on an Mg-rich silicocarbonatitic melt composition from groundmass mineralogy and bulk compositions. Can. Mineral. 46, 1043–1061. https://doi.org/10.3749/canmin.46.4.1043.
Nielsen, T.F.D., Jensen, S.M., Secher, K., Sand, K.K., 2009. Distribution of kimberlite and aillikite in the Diamond Province of southern West Greenland: a regional perspective based on groundmass mineral chemistry and bulk compositions. Lithos 112, 358–371. https://doi.org/10.1016/j.lithos.2009.05.035.
Nowell, G.M., Pearson, D.G., Bell, D.R., Carlson, R.W., Smith, C.B., Kempton, P.D., Noble, S.R., 2004. Hf isotope systematics of kimberlites and their megacrysts: New constraints on their source regions. J. Petrol. 45, 1583–1612. https://doi.org/10.1093/petrology/egh024.
Nutman, A.P., Friend, C.R.L., Barker, S.L.L., McGregor, V.R., 2004. Inventory and assessment of Palaeoarchaean gneiss terrains and detrital zircons in southern West Greenland. Precambrian Res. 135, 281–314. https://doi.org/10.1016/j.precamres.2004.09.002.
Parthasarathy, G., Chetty, T.R.K., Haggerty, S.E., 2002. Thermal stability and spectroscopic studies of zemkorite: a carbonate from the Venkatampalle kimberlite of southern India. Am. Mineral. 87, 1384–1389.
Paul, D.K., Buckley, F., Nixon, P.H., 1976. Fluorine and chlorine geochemistry of kimberlites. Chem. Geol. 17.
Pearce, J.A., Peate, D.W., 1995. Tectonic implications on the composition of volcanic arc magmas. Annu. Rev. Earth Planet. Sci. 23, 251–285.
Pearson, D.G., Carlson, R.W., Shirey, S.B., Boyd, F.R., Nixon, P.H., 1995a. Stabilisation of Archaean lithospheric mantle: a ReOs isotope study of peridotite xenoliths from the Kaapvaal craton. Earth Planet. Sci. Lett. 134, 341–357. https://doi.org/10.1016/0012-821X(95)00125-V.
Pearson, D.G., Shirey, S.B., Carlson, R.W., Boyd, F.R., Pokhilenko, N.P., Shimizu, N., 1995b. Re-Os, Sm-Nd, and Rb-Sr isotope evidence for thick Archaean lithospheric mantle beneath the Siberian craton modified by multistage metasomatism. Geochim. Cosmochim. Acta 59, 959–977. https://doi.org/10.1016/0016-7037(95)00014-3.
Pearson, D.G., Woodhead, J., Janney, P.E., 2019. Kimberlites as Geochemical Probes of Earth's Mantle. Elements 15, 387–392. https://doi.org/10.2138/gselements.15.6.387.
Portnyagin, M., Duggen, S., Hauff, F., Mironov, N., Bindeman, I., Thirlwall, M., Hoernle, K., 2015. Geochemistry of the late Holocene rocks from the Tolbachik volcanic field, Kamchatka: Quantitative modelling of subduction-related open magmatic systems. J. Volcanol. Geotherm. Res. 307, 133–155. https://doi.org/10.1016/j.jvolgeores.2015.08.015.
Rooney, T., Girard, G., Tappe, S., 2020. The impact on mantle olivine resulting from carbonated silicate melt interaction. Contrib. Mineral. Petrol. 175, 1–15. https://doi.org/10.1007/s00410-020-01694-0.
Rudnick, R.L., McDonough, W.F., Chappell, B.W., 1993. Carbonatite metasomatism in the northern Tanzanian mantle: petrographic and geochemical characteristics. Earth Planet. Sci. Lett. 114, 463–475. https://doi.org/10.1016/0012-821X(93)90076-L.
Schauble, E.A., Rossman, G.R., Taylor, H.P.J., 2003. Theoretical estimates of equilibrium chlorine-isotope fractionations. Geochim. Cosmochim. Acta. 67, 3267–3281. https://doi.org/10.1016/S0016-7037(00)01375-3.
Sharp, Z.D., Barnes, J.D., Brearley, A.J., Chaussidon, M., Fischer, T.P., Kamenetsky, V.S., 2007. Chlorine isotope homogeneity of the mantle, crust and carbonaceous chondrites. Nature 446, 1062–1065. https://doi.org/10.1038/nature05748.
Sharp, Z.D., Mercer, J.A., Jones, R.H., Brearley, A.J., Selverstone, J., Bekker, A., Stachel, T., 2013. The chlorine isotope composition of chondrites and Earth. Geochim. Cosmochim. Acta 107, 189–204. https://doi.org/10.1016/j.gca.2013.01.003.
Simon, N.S.C., Carlson, R.W., Pearson, D.G., Davies, G.R., 2007. The origin and evolution of the Kaapvaal Cratonic Lithospheric Mantle. J. Petrol. 48, 589–625. https://doi.org/10.1093/petrology/egl074.
Smart, K.A., Tappe, S., Ishikawa, A., Pfänder, J.A., Stracke, A., 2019. K-rich hydrous mantle lithosphere beneath the Ontong Java Plateau: significance for the genesis of oceanic basalts and Archean continents. Geochim. Cosmochim. Acta 248, 311–342. https://doi.org/10.1016/j.gca.2019.01.013.
Smith, C.B., 1983. Pb, Sr and Nd isotopic evidence for sources of southern African cretaceous kimberlites. Nature 304, 51–54. https://doi.org/10.1038/304051a0.
Smith, J.V., Delaney, J.S., Hervig, R.L., Dawson, J.B., 1981. Storage of F and Cl in the upper mantle: geochemical implications. Lithos 14, 133–147. https://doi.org/10.1016/0024-4937(81)90050-5.
Sparks, R.S.J., Brooker, R.A., Field, M., Kavanagh, J., Schumacher, J.C., Walter, M.J., White, J., 2009. The nature of erupting kimberlite melts. Lithos 112, 429–438. https://doi.org/10.1016/j.lithos.2009.05.032.
Stamm, N., Schmidt, M.W., 2017. Asthenospheric kimberlites: Volatile contents and bulk compositions at 7 GPa. Earth Planet. Sci. Lett. 474, 309–321. https://doi.org/10.1016/j.epsl.2017.06.037.
Stead, C.V., Tomlinson, E.L., Kamber, B.S., Babechuk, M.G., McKenna, C.A., 2017. Rare earth element determination in olivine by laser ablation-quadrupole-ICP-MS: an analytical strategy and applications. Geostand. Geoanal. Res. 41, 197–212. https://doi.org/10.1111/ggr.12157.
Steenfelt, A., Hollis, J.A., Secher, K., 2006. The Tikiusaaq carbonatite: a new Mesozoic intrusive complex in southern West Greenland. Geol. Survey Denmark Greenland Bull. 41–44.

Tachibana, Y., Kaneoka, I., Gaffney, A., Upton, B., 2006. Ocean-island basalt-like source of kimberlite magmas from West Greenland revealed by high 3He/4He ratios. Geology 34, 273–276. https://doi.org/10.1130/G22201.1.

Tappe, S., Foley, S.F., Jenner, G.A., Kjarsgaard, B.A., 2005. Integrating ultramafic lamprophyres into the IUGS classification of igneous rocks: Rationale and implications. J. Petrol. 46, 1893–1900. https://doi.org/10.1093/petrology/egi039.

Tappe, S., Foley, S.F., Stracke, A., Romer, R.L., Kjarsgaard, B.A., Heaman, L.M., Joyce, N., 2007. Craton reactivation on the Labrador Sea margins: 40Ar/39Ar age and Sr-Nd-Hf-Pb isotope constraints from alkaline and carbonatite intrusives. Earth Planet. Sci. Lett. 256, 433–454. https://doi.org/10.1016/j.epsl.2007.01.036.

Tappe, S., Steenfelt, A., Heaman, L.M., Simonetti, A., 2009. The newly discovered Jurassic Tikiusaaq carbonatite-aillikite occurrence, West Greenland, and some remarks on carbonatite–kimberlite relationships. Lithos 112, 385–399. https://doi.org/10.1016/j.lithos.2009.03.002.

Tappe, S., Pearson, D.G., Nowell, G., Nielsen, T., Milstead, P., Muehlenbachs, K., 2011a. A fresh isotopic look at Greenland kimberlites: Cratonic mantle lithosphere imprint on deep source signal. Earth Planet. Sci. Lett. 305, 235–248. https://doi.org/10.1016/j.epsl.2011.03.005.

Tappe, S., Smart, K.A., Pearson, D.G., Steenfelt, A., Simonetti, A., 2011b. Craton formation in late archean subduction zones revealed by first Greenland eclogites. Geology 39, 1103–1106. https://doi.org/10.1130/G32348.1.

Tappe, S., Steenfelt, A., Nielsen, T., 2012. Asthenospheric source of Neoproterozoic and Mesozoic kimberlites from the North Atlantic craton, West Greenland: New high-precision U-Pb and Sr-Nd isotope data on perovskite. Chem. Geol. 320–321, 113–127. https://doi.org/10.1016/j.chemgeo.2012.05.026.

Tappe, S., Graham Pearson, D., Kjarsgaard, B.A., Nowell, G., Dowall, D., 2013. Mantle transition zone input to kimberlite magmatism near a subduction zone: Origin of anomalous Nd-Hf isotope systematics at Lac de Gras, Canada. Earth Planet. Sci. Lett. 371–372, 235–251. https://doi.org/10.1016/j.epsl.2013.03.039.

Tappe, S., Romer, R.L., Stracke, A., Steenfelt, A., Smart, K.A., Muehlenbachs, K., Torsvik, T.H., 2017. Sources and mobility of carbonate melts beneath cratons, with implications for deep carbon cycling, metasomatism and rift initiation. Earth Planet. Sci. Lett. 466, 152–167. https://doi.org/10.1016/j.epsl.2017.03.011.

Tappe, S., Smart, K., Torsvik, T., Massuyeau, M., de Wit, M., 2018. Geodynamics of kimberlites on a cooling Earth: Clues to plate tectonic evolution and deep volatile cycles. Earth Planet. Sci. Lett. 484, 1–14. https://doi.org/10.1016/j.epsl.2017.12.013.

Tappe, S., Budde, G., Stracke, A., Wilson, A., Kleine, T., 2020a. The tungsten-182 record of kimberlites above the African superplume: Exploring links to the core-mantle boundary. Earth Planet. Sci. Lett. 547, 116473. https://doi.org/10.1016/j.epsl.2020.116473.

Tappe, S., Stracke, A., van Acken, D., Strauss, H., Luguet, A., 2020b. Origins of kimberlites and carbonatites during continental collision – Insights beyond decoupled Nd-Hf isotopes. Earth Sci. Rev. 208, 103287. https://doi.org/10.1016/j.earscirev.2020.103287.

Ubide, T., Guyett, P.C., Kenny, G.G., O'Sullivan, E.M., Ames, D.E., Petrus, J.A., Riggs, N., Kamber, B.S., 2017. Protracted volcanism after large impacts: evidence from the Sudbury impact basin. J. Geophys. Res. 122, 701–728. https://doi.org/10.1002/2016JE005085.

van Acken, D., Luguet, A., Pearson, D.G., Nowell, G.M., Fonseca, R.O.C., Nagel, T.J., Schulz, T., 2017. Mesoarchean melting and Neoarchean to Paleoproterozoic metasomatism during the formation of the cratonic mantle keel beneath West Greenland. Geochim. Cosmochim. Acta 203, 37–53. https://doi.org/10.1016/j.gca.2017.01.006.

Veksler, I.V., Petibon, C., Jenner, G.A., Dorfman, A.M., Dingwell, D.B., 1998. Trace element partitioning in immiscible silicate-carbonate liquid systems: an initial experimental study using a centrifuge autoclave. J. Petrol. 39, 2095–2104. https://doi.org/10.1093/petroj/39.11-12.2095.

Veksler, I.V., Dorfman, A.M., Dulski, P., Kamenetsky, V.S., Danyushevsky, L.V., Jeffries, T., Dingwell, D.B., 2012. Partitioning of elements between silicate melt and immiscible fluoride, chloride, carbonate, phosphate and sulfate melts, with implications to the origin of natrocarbonatite. Geochim. Cosmochim. Acta 79, 20–40. https://doi.org/10.1016/j.gca.2011.11.035.

Wang, C., Liu, Y., Min, N., Zong, K., Hu, Z., Gao, S., 2016. Paleo-Asian oceanic subduction-related modification of the lithospheric mantle under the North China Craton: evidence from peridotite xenoliths in the Datong basalts. Lithos 261, 109–127. https://doi.org/10.1016/j.lithos.2015.12.011.

Watkinson, W.H., Chao, G.Y., 1973. Shortite in Kimberlite from the Upper Canada Gold Mine, Ontario Author (s): David H. Watkinson and G. Y. Chao Published by: The University of Chicago Press Stable URL: http://www.jstor.org/stable/30061149. J. Geol. 81, 229–233.

Webster, J.D., Baker, D.R., Aiuppa, A., 2018. Halogens in Mafic and Intermediate-Silica Content Magmas. In: Harlov, D.E., Aranovich, L. (Eds.), The Role of Halogens in Terrestrial and Extraterrestrial Geochemical Processes. Springer, Cham, pp. 307–430.

Weiss, Y., McNeill, J., Pearson, D.G., Nowell, G.M., Ottley, C.J., 2015. Highly saline fluids from a subducting slab as the source for fluid-rich diamonds. Nature 524, 339–342. https://doi.org/10.1038/nature14857.

Wilson, M.R., Kjarsgaard, B.A., Taylor, B., 2007. Stable isotope composition of magmatic and deuteric carbonate phases in hypabyssal kimberlite, Lac de Gras field, Northwest Territories, Canada. Chem. Geol. 242, 435–454. https://doi.org/10.1016/j.chemgeo.2007.05.002.

Wittig, N., Webb, M., Pearson, D.G., Dale, C.W., Ottley, C.J., Hutchison, M., Jensen, S.M., Luguet, A., 2010. Formation of the North Atlantic Craton: timing and mechanisms constrained from Re-Os isotope and PGE data of peridotite xenoliths from S.W. Greenland. Chem. Geol. 276, 166–187. https://doi.org/10.1016/j.chemgeo.2010.06.002.

Woolley, A.R., Kjarsgaard, B.A., 2008. Paragenetic types of carbonatite as indicated by the diversity and relative abundances of associated silicate rocks: evidence from a global database. Can. Mineral. 46, 741–752. https://doi.org/10.3749/canmin.46.4.741.

Yaxley, G.M., Crawford, A.J., Green, D.H., 1991. Evidence for carbonatite metasomatism in spinel peridotite xenoliths from western Victoria, Australia. Earth Planet. Sci. Lett. 107, 305–317. https://doi.org/10.1016/0012-821X(91)90078-V.

Zaitsev, A.N., Keller, J., 2006. Mineralogical and chemical transformation of Oldoinyo Lengai natrocarbonatites, Tanzania. Lithos 91, 191–207. https://doi.org/10.1016/j.lithos.2006.03.018.